

ENTROPY STABLE, POSITIVE DGSEM WITH SHARP RESOLUTION OF MATERIAL INTERFACES FOR A 4×4 TWO-PHASE FLOW SYSTEM: A LEGACY FROM THREE-POINT SCHEMES

FLORENT RENAC*

Abstract. This work concerns the numerical approximation of the multicomponent compressible Euler system for a mixture of immiscible fluids in multiple space dimensions and its contribution is twofold. We first derive an entropy stable, positive and accurate three-point finite volume scheme using relaxation-based approximate Riemann solvers from Bouchut [Nonlinear stability of finite volume methods for hyperbolic conservation laws and well-balanced schemes for sources, *Frontiers in Mathematics*, Birkhauser, 2004] and Coquel and Perthame [*SIAM J. Numer. Anal.*, 35 (1998), pp. 2223–2249]. Then, we extend these results to the high-order discontinuous Galerkin spectral element method (DGSEM) based on collocation of quadrature and interpolation points [Kopriva and Gassner, *J. Sci. Comput.*, 44 (2010), pp.136–155]. The method relies on the framework introduced by Fisher and Carpenter [*J. Comput. Phys.*, 252 (2013), pp. 518–557] and Gassner [*SIAM J. Sci. Comput.*, 35 (2013), pp. A1233–A1253] where we replace the physical fluxes by entropy conservative numerical fluxes [Tadmor, *Math. Comput.*, 49 (1987), pp. 91–103] in the integral over discretization elements, while entropy stable numerical fluxes are used at element interfaces. Time discretization is performed with a strong-stability preserving Runge-Kutta scheme. We design two-point numerical fluxes satisfying the Tadmor’s entropy conservation condition and use the numerical flux from the three-point scheme as entropy stable flux. We derive conditions on the numerical parameters to guaranty a semi-discrete entropy inequality as well as positivity of the fully discrete DGSEM scheme at any approximation order. The scheme is also accurate in the sense that the solution at interpolation points is exact for stationary contact waves and material interfaces. Numerical experiments in one and two space dimensions on flows with discontinuous solutions support the conclusions of our analysis and highlight stability, robustness and high resolution of the scheme.

Key words. Compressible multicomponent flows, entropy stable scheme, discontinuous Galerkin method, summation-by-parts, relaxation scheme

AMS subject classifications. 65M12, 65M70, 76T10

1. Introduction. The accurate and robust simulation of compressible flows with material interfaces separating fluids with different properties is of strong significance in many engineering applications (e.g., combustion in propulsion systems, explosive detonation products) and scientific applications (e.g., flow instabilities, chemical reactions, phase changes). These flows may involve nonlinear waves such as shock and rarefaction waves, contact waves, material interfaces separating different fluids, and their interactions which usually trigger phenomena leading to small scale flow structures. The discussion in this paper focuses on the nonlinear analysis of a high-order discretization of the multicomponent compressible Euler system for a mixture of immiscible fluids in multiple space dimensions. Such system falls into the category of diffuse interface models where the PDEs for the mixture are supplemented with evolution equations for the mass fractions of the different phases [49]. The design of high-order discretizations of such flows based on interface capturing methods has been the subject of numerous works. Though not exhaustive, we refer to the works on finite differences [38, 36, 40, 7], finite volume methods [35, 31], or discontinuous Galerkin (DG) methods [56, 29, 53] and references therein.

In this context, we consider the discontinuous Galerkin spectral element method (DGSEM) based on the collocation between interpolation and quadrature points [37]. Using diagonal norm summation-by-parts (SBP) operators and the entropy conservative numerical fluxes from Tadmor [51], semi-discrete entropy conservative finite-difference and spectral collocation schemes have been

*DAAA, ONERA, Université Paris Saclay, F-92322 Châtillon, France (florent.renac@onera.fr).

derived in [8, 9] for nonlinear conservation laws. Entropy stable DGSEM for the compressible Euler equations on hexahedral [24] and triangular [14] meshes have been proposed by using the same framework. The particular form of the SBP operators allows to take into account the numerical quadratures that approximate integrals in the numerical scheme compared to other techniques that require their exact evaluation to satisfy the entropy inequality [33, 30]. The DGSEM thus provides a general framework for the design of entropy stable schemes for nonlinear systems of conservation laws. An entropy stable DGSEM for the discretization of general nonlinear hyperbolic systems in nonconservative form has been introduced in [48] and applied to two-phase flow models [48, 16]. Numerical experiments in [24, 54, 14, 48, 16] highlight the benefits on stability and robustness of the computations, though this not guarantees to preserve neither the entropy stability at the fully discrete level, nor positivity of the numerical solution. Designs of fully discrete entropy stable and positive DGSEM have been proposed in [19, 20, 46, 47, 48].

In the context of high-order schemes, a common way to design entropy stable numerical fluxes in the sense of Tadmor [51] is to derive entropy conservative numerical fluxes to which one adds ad-hoc dissipation [52, 22, 9, 24, 55, 48, 16, 11]. Nevertheless, this may cause difficulties to derive further properties of the scheme, such as preservation of invariant domains, bound preservation, or exact resolution of isolated shocks and contacts, because the numerical flux may involve intricate operations of its arguments [32, 11]. These properties are however important for the robustness and accuracy of the scheme. Besides, for smooth solutions or large scale oscillations around discontinuities the DG approximation is known to become less sensitive to the numerical flux as the scheme accuracy increases [43, 44], but this is no longer the case when small scale flow features are involved and the numerical flux has a strong effect on their resolution [39, 12]. One has therefore to pay a lot of attention in the design of the numerical fluxes at interfaces. In the present work, we adopt a different strategy and first design an entropy stable, positive and accurate three-point scheme and then use it as a building block to define an entropy stable, positive and accurate DGSEM.

The difficulty in the design of an entropic and positive three-point scheme for the multicomponent compressible Euler system lies in the fact that the thermodynamic properties of the mixture depend on the mass fractions of the different phases. In [18] a relaxation technique is applied to the multicomponent Euler system which allows the use of monocomponent entropic schemes for each component. However, this technique does not hold for the separated fluid mixture in Eulerian coordinates under consideration in this work. Here, we consider the energy relaxation technique introduced in [17] for the approximation of the monocomponent compressible Euler equations with general equation of states. The method allows the design of entropic and positive numerical schemes by using classical numerical fluxes for polytropic gases. We extend this method to our model and show how to define an entropic numerical scheme from a scheme for the polytropic gas dynamics with additional equations for the mass fraction and relaxation energy. This latter scheme uses the entropic and positive approximate Riemann solver based on pressure relaxation and introduced in [4]. Relaxation schemes circumvent the difficulties in the treatment of nonlinearities associated to the equation of state by approximating the nonlinear system with a consistent linearly degenerate (LD) enlarged system with stiff relaxation source terms [34, 15, 10]. The entropy of the energy relaxation approximation of our model satisfies a variational principle but is not strictly convex which prevents to apply classical stability theorems [13]. The use of the pressure relaxation approximation however circumvents this difficulty mainly because of its LD character and results in entropy stability for our model.

The numerical flux is used in the DGSEM at mesh interfaces, while an entropy conservative numerical flux is used within the discretization elements resulting in a semi-discrete entropy stable

scheme. We prove that the discrete scheme with explicit time integration exactly captures stationary contacts and material interfaces at interpolation points. We further derive conditions on the time step to keep positivity of the mean value of the numerical solution in discretization elements. This is achieved by extending the framework introduced in [57] for Cartesian meshes to unstructured meshes with straight-sided quadrangles. We formulate the DGSEM for the cell-averaged solution as a convex combination of positive quantities under a CFL condition by using results from [41]. We finally apply a posteriori limiters [57] that extend the positivity to nodal values within elements.

The paper is organized as follows. Section 2 presents the multicomponent compressible Euler system under consideration and some of its properties. We derive the entropy conservative two-point numerical flux in subsection 3.1, while in subsection 3.2 we recall some properties of three-point schemes. We derive an entropy stable relaxation-based three-point scheme in section 4 that we then use as building block for the DGSEM introduced in section 5. We analyze the properties of the fully discrete DGSEM in section 6. The results are assessed by numerical experiments in one and two space dimensions in section 7 and concluding remarks about this work are given in section 8.

2. Model problem. Let $\Omega \subset \mathbb{R}^d$ be a bounded domain in d space dimensions, we consider the IBVP described by the multicomponent compressible Euler system for a mixture of two immiscible fluids. The model is known as the homogeneous relaxation model (HRM) [1]. We do not consider relaxation processes that come from some chemical reactions and the problem takes the form

$$(2.1a) \quad \partial_t \mathbf{u} + \nabla \cdot \mathbf{f}(\mathbf{u}) = 0, \quad \text{in } \Omega \times (0, \infty),$$

$$(2.1b) \quad \mathbf{u}(\cdot, 0) = \mathbf{u}_0(\cdot), \quad \text{in } \Omega,$$

with some boundary conditions to be prescribed on $\partial\Omega$ (see section 7). Here,

$$(2.2) \quad \mathbf{u} = (\rho Y, \rho, \rho \mathbf{v}^\top, \rho E)^\top, \quad \mathbf{f}(\mathbf{u}) = (\rho Y \mathbf{v}, \rho \mathbf{v}, \rho \mathbf{v} \mathbf{v}^\top + \mathbf{p} \mathbf{I}, (\rho E + \mathbf{p}) \mathbf{v})^\top,$$

denote the conserved variables and the convective fluxes with Y the mass fraction of the first fluid; ρ , \mathbf{v} in \mathbb{R}^d , and E are the density, velocity vector, and total specific energy of the mixture, respectively. The mixture quantities are defined from quantities of both phases $i = 1, 2$ through

$$\rho = \alpha \rho_1 + (1 - \alpha) \rho_2, \quad \rho E = \alpha \rho_1 E_1 + (1 - \alpha) \rho_2 E_2, \quad \mathbf{p} = \alpha \mathbf{p}_1(\rho_1, e_1) + (1 - \alpha) \mathbf{p}_2(\rho_2, e_2),$$

where $E_{i=1,2} = e_i + \frac{\mathbf{v} \cdot \mathbf{v}}{2}$ and $\alpha = \rho Y / \rho_1$ is the void fraction. The total energy of the mixture reads

$$(2.3) \quad \rho E = \alpha \rho_1 \left(e_1 + \frac{\mathbf{v} \cdot \mathbf{v}}{2} \right) + (1 - \alpha) \rho_2 \left(e_2 + \frac{\mathbf{v} \cdot \mathbf{v}}{2} \right) = \rho e + \rho \frac{\mathbf{v} \cdot \mathbf{v}}{2}.$$

where $\rho e = \alpha \rho_1 e_1 + (1 - \alpha) \rho_2 e_2$ denotes the internal energy of the mixture per unit volume.

Equations (2.1) are supplemented with polytropic ideal gas equations of states:

$$(2.4) \quad \mathbf{p}_i(\rho_i, e_i) = (\gamma_i - 1) \rho_i e_i, \quad e_i = C_{v_i} T_i, \quad i = 1, 2,$$

where $\gamma_i = C_{p_i} / C_{v_i} > 1$ is the ratio of specific heats which are assumed to be positive constants of the model. The HRM model assumes thermal and mechanical equilibria:

$$(2.5) \quad T_1(\rho_1, e_1) = T_2(\rho_2, e_2) =: T(Y, \rho, e), \quad \mathbf{p}_1(\rho_1, e_1) = \mathbf{p}_2(\rho_2, e_2) =: \mathbf{p}(Y, \rho, e),$$

thus leading to

$$(2.6a) \quad e(Y, T) = C_v(Y) T,$$

$$(2.6b) \quad \mathbf{p}(Y, \rho, e) = (\gamma(Y) - 1) \rho e = \rho r(Y) T(Y, \rho, e),$$

with

$$(2.7) \quad r(Y) = C_p(Y) - C_v(Y), \quad C_p(Y) = Y C_{p_1} + (1 - Y) C_{p_2}, \quad C_v(Y) = Y C_{v_1} + (1 - Y) C_{v_2},$$

and

$$(2.8) \quad \gamma(Y) = \frac{C_p(Y)}{C_v(Y)}.$$

Note that due to (2.4) and (2.5) we have

$$(2.9) \quad \rho r(Y) = \rho_i r_i, \quad r_i := C_{p_i} - C_{v_i}, \quad i = 1, 2.$$

System (2.1a) is hyperbolic in the direction \mathbf{n} in \mathbb{R}^d over the set of states

$$(2.10) \quad \Omega^a = \{\mathbf{u} \in \mathbb{R}^{d+3} : 0 \leq Y \leq 1, \rho > 0, e = E - \frac{\mathbf{v} \cdot \mathbf{v}}{2} > 0\},$$

with eigenvalues $\lambda_1 = \mathbf{v} \cdot \mathbf{n} - c \leq \lambda_2 = \dots = \lambda_{d+2} = \mathbf{v} \cdot \mathbf{n} \leq \lambda_{d+3} = \mathbf{v} \cdot \mathbf{n} + c$, where $\lambda_{1,5}$ are associated to genuinely nonlinear fields and $\lambda_{2 \leq i \leq d+2}$ to LD fields. The sound speed is defined by

$$(2.11) \quad c(Y, e) = \sqrt{\gamma(Y)(\gamma(Y) - 1)e}.$$

Without loss of generality, we assume that $\gamma_1 > \gamma_2$ which induces that $\gamma'(\cdot) > 0$ and thus

$$(2.12) \quad \gamma_2 \leq \gamma(Y) \leq \gamma_1 \quad \forall 0 \leq Y \leq 1.$$

Solutions to (2.1) should satisfy the entropy inequality

$$(2.13) \quad \partial_t \eta(\mathbf{u}) + \nabla \cdot \mathbf{q}(\mathbf{u}) \leq 0,$$

for the entropy – entropy flux pair

$$(2.14) \quad \eta(\mathbf{u}) = -\rho s(\mathbf{u}), \quad \mathbf{q}(\mathbf{u}) = -\rho s(\mathbf{u}) \mathbf{v}, \quad s \equiv Y s_1 + (1 - Y) s_2,$$

where the specific entropies are defined by the second law of thermodynamics and using (2.5):

$$(2.15) \quad T ds_i = de_i - \frac{p}{\rho_i^2} d\rho_i, \quad i = 1, 2,$$

and read $s_i(\rho_i, e_i) = C_{v_i} \ln\left(\frac{e_i}{\rho_i^{\gamma_i-1}}\right) + s_i^\infty$ with s_i^∞ an additive constant, so

$$(2.16) \quad s(Y, \rho, e) = C_v(Y) \ln\left(\frac{e}{\rho^{\gamma(Y)-1}}\right) + K(Y),$$

$$K(Y) = Y \left(C_{v_1} \ln\left(\frac{C_{v_1}}{C_v(Y)} \left(\frac{r_1}{r(Y)}\right)^{\gamma_1-1}\right) + s_1^\infty \right) + (1 - Y) \left(C_{v_2} \ln\left(\frac{C_{v_2}}{C_v(Y)} \left(\frac{r_2}{r(Y)}\right)^{\gamma_2-1}\right) + s_2^\infty \right).$$

Using the differential forms (2.15) and $\theta = \frac{1}{T}$ is the inverse temperature, the entropy variables read

$$(2.17) \quad \boldsymbol{\eta}'(\mathbf{u}) = \begin{pmatrix} s_2 - s_1 + C_{p_1} - C_{p_2} \\ C_{p_2} - s_2 - \frac{\mathbf{v} \cdot \mathbf{v}}{2} \theta \\ \theta \mathbf{v} \\ -\theta \end{pmatrix},$$

and the entropy potential is easily obtained:

$$(2.18) \quad \boldsymbol{\psi}(\mathbf{u}) := \mathbf{f}(\mathbf{u})^\top \boldsymbol{\eta}'(\mathbf{u}) - \mathbf{q}(\mathbf{u}) = r(Y) \rho \mathbf{v}.$$

3. Two-point numerical fluxes and associated finite volume schemes.

3.1. Entropy conservative and entropy stable numerical fluxes. In the following, we design numerical fluxes for the space discretization of (2.1). We adopt the usual terminology from [51] and denote by *entropy conservative* for the pair (η, \mathbf{q}) in (2.13), a numerical flux \mathbf{h}_{ec} satisfying

$$(3.1) \quad \llbracket \boldsymbol{\eta}'(\mathbf{u}) \rrbracket \cdot \mathbf{h}_{ec}(\mathbf{u}^-, \mathbf{u}^+, \mathbf{n}) = \llbracket \boldsymbol{\psi}(\mathbf{u}) \cdot \mathbf{n} \rrbracket \quad \forall \mathbf{u}^\pm \in \Omega^a,$$

where $\llbracket a \rrbracket = a^+ - a^-$ denotes the jump operator of a at a given point \mathbf{x} and $a^\pm = \lim_{\epsilon \downarrow 0} a(\mathbf{x} \pm \epsilon \mathbf{n})$. Entropy stability of the DGSEM also requires the flux to be symmetric in the sense $\mathbf{h}_{ec}(\mathbf{u}^-, \mathbf{u}^+, \mathbf{n}) = \mathbf{h}_{ec}(\mathbf{u}^+, \mathbf{u}^-, \mathbf{n})$ [8, 14]. Then, a numerical flux \mathbf{h} will be *entropy stable* when

$$(3.2) \quad \llbracket \boldsymbol{\eta}'(\mathbf{u}) \rrbracket \cdot \mathbf{h}(\mathbf{u}^-, \mathbf{u}^+, \mathbf{n}) \leq \llbracket \boldsymbol{\psi}(\mathbf{u}) \cdot \mathbf{n} \rrbracket \quad \forall \mathbf{u}^\pm \in \Omega^a.$$

Both numerical fluxes are assumed to be Lipschitz continuous, consistent:

$$(3.3) \quad \mathbf{h}_{ec}(\mathbf{u}, \mathbf{u}, \mathbf{n}) = \mathbf{h}(\mathbf{u}, \mathbf{u}, \mathbf{n}) = \mathbf{f}(\mathbf{u}) \cdot \mathbf{n} \quad \forall \mathbf{u} \in \Omega^a,$$

and conservative:

$$(3.4) \quad \mathbf{h}_{ec}(\mathbf{u}^-, \mathbf{u}^+, \mathbf{n}) = -\mathbf{h}_{ec}(\mathbf{u}^+, \mathbf{u}^-, -\mathbf{n}), \quad \mathbf{h}(\mathbf{u}^-, \mathbf{u}^+, \mathbf{n}) = -\mathbf{h}(\mathbf{u}^+, \mathbf{u}^-, -\mathbf{n}) \quad \forall \mathbf{u}^\pm \in \Omega^a.$$

In this work we propose numerical fluxes that satisfy these properties.

PROPOSITION 1. *The following numerical flux is a symmetric, consistent, and entropy conservative (3.1) numerical flux for the HRM model (2.1) and pair (η, \mathbf{q}) in (2.13):*

$$(3.5) \quad \mathbf{h}_{ec}(\mathbf{u}^-, \mathbf{u}^+, \mathbf{n}) = \begin{pmatrix} h_{\rho Y}(\mathbf{u}^-, \mathbf{u}^+, \mathbf{n}) \\ h_{\rho}(\mathbf{u}^-, \mathbf{u}^+, \mathbf{n}) \\ h_{\rho}(\mathbf{u}^-, \mathbf{u}^+, \mathbf{n}) \bar{\mathbf{v}} + \frac{\bar{\rho} \theta}{\bar{\theta}} \mathbf{n} \\ \frac{C_{v_1} - C_{v_2}}{\bar{\theta}} h_{\rho Y}(\mathbf{u}^-, \mathbf{u}^+, \mathbf{n}) + \left(\frac{C_{v_2}}{\bar{\theta}} + \frac{\mathbf{v}^- \cdot \mathbf{v}^+}{2} \right) h_{\rho}(\mathbf{u}^-, \mathbf{u}^+, \mathbf{n}) + \frac{\bar{\rho} \theta}{\bar{\theta}} \bar{\mathbf{v}} \cdot \mathbf{n} \end{pmatrix}$$

with $h_{\rho Y}(\mathbf{u}^-, \mathbf{u}^+, \mathbf{n}) = \frac{r_2(\widehat{\rho_2} - \bar{\rho})}{r_1 - r_2} \bar{\mathbf{v}} \cdot \mathbf{n}$ and $h_{\rho}(\mathbf{u}^-, \mathbf{u}^+, \mathbf{n}) = \widehat{\rho} \bar{\mathbf{v}} \cdot \mathbf{n}$, where $\widehat{a} = \frac{\llbracket a \rrbracket}{\llbracket \ln a \rrbracket}$ and $\bar{a} = \frac{a^+ + a^-}{2}$ denote the logarithmic mean [32] and average operator.

Proof. Symmetry follows from the symmetry of the logarithmic mean and average operator. Then, observe that $h_{\rho Y}(\mathbf{u}, \mathbf{u}, \mathbf{n}) = \frac{r_2(\rho_2 - \rho)}{r_1 - r_2} \mathbf{v} \cdot \mathbf{n} \stackrel{(2.6)}{=} \frac{(r(Y) - r_2)\rho}{r_1 - r_2} \mathbf{v} \cdot \mathbf{n} \stackrel{(2.7)}{=} \rho Y \mathbf{v} \cdot \mathbf{n}$, thus consistency follows. Now we expand

$$\llbracket s_i \rrbracket_{i=1,2} \stackrel{(2.15)}{=} -C_{v_i} \llbracket \ln \theta \rrbracket - r_i \llbracket \ln \rho_i \rrbracket, \quad \llbracket \boldsymbol{\psi}(\mathbf{u}) \rrbracket \stackrel{(2.18)}{\stackrel{(2.9)}{=}} \llbracket r_2 \rho_2 \mathbf{v} \cdot \mathbf{n} \rrbracket = r_2 (\bar{\rho}_2 \llbracket \mathbf{v} \rrbracket + \llbracket \rho_2 \rrbracket \bar{\mathbf{v}}) \cdot \mathbf{n},$$

and using short notations

$$\begin{aligned} \llbracket \boldsymbol{\eta}'(\mathbf{u}) \rrbracket \cdot \mathbf{h}_{ec}(\mathbf{u}^-, \mathbf{u}^+, \mathbf{n}) &= \llbracket (C_{v_1} - C_{v_2}) \ln \theta + (r_1 - r_2) \ln \rho_2 \rrbracket h_{\rho Y} \\ &\quad + \llbracket C_{v_2} \ln \theta + r_2 \ln \rho_2 - \frac{\mathbf{v}^- \cdot \mathbf{v}^+}{2} \theta \rrbracket h_{\rho} + \llbracket \theta \mathbf{v} \rrbracket \cdot \mathbf{h}_{\rho \mathbf{v}} - \llbracket \theta \rrbracket h_{\rho E}, \end{aligned}$$

and after some algebraic manipulations we conclude by imposing that (3.1) must hold for all $\llbracket \rho \rrbracket$, $\llbracket \mathbf{v} \rrbracket$, and $\llbracket \theta \rrbracket$. \square

Remark 2. Due to the particular form of the convective terms in the momentum equations, it can be shown that the numerical flux (3.5) is formally kinetic energy preserving [11].

3.2. Entropy stable and positive finite volume schemes. We first consider three-point numerical schemes of the form

$$(3.6) \quad \mathbf{U}_j^{n+1} = \mathbf{U}_j^n - \frac{\Delta t}{\Delta x} (\mathbf{h}(\mathbf{U}_j^n, \mathbf{U}_{j+1}^n, \mathbf{n}) - \mathbf{h}(\mathbf{U}_{j-1}^n, \mathbf{U}_j^n, \mathbf{n})), \quad 0 < \frac{\Delta t}{\Delta x} \max_{j \in \mathbb{Z}} |\lambda(\mathbf{U}_j^n)| \leq \alpha_{max},$$

for the discretization of (2.1a) in one space dimension. Here, \mathbf{U}_j^n approximates the averaged solution in the j -th cell at time $t^{(n)}$, Δt and Δx are the time and space steps, $|\lambda(\cdot)|$ corresponds to the maximum absolute value of the wave speeds, and $\alpha_{max} \leq 1$ corresponds to a bound on $\frac{\Delta t}{\Delta x}$ which depends on the numerical flux. The scheme (3.6) is said to be entropy stable for the pair (η, \mathbf{q}) in (2.13) if it satisfies the inequality

$$(3.7) \quad \eta(\mathbf{U}_j^{n+1}) - \eta(\mathbf{U}_j^n) + \frac{\Delta t}{\Delta x} (Q(\mathbf{U}_j^n, \mathbf{U}_{j+1}^n, \mathbf{n}) - Q(\mathbf{U}_{j-1}^n, \mathbf{U}_j^n, \mathbf{n})) \leq 0,$$

with some consistent entropy numerical flux $Q(\mathbf{u}, \mathbf{u}, \mathbf{n}) = \mathbf{q}(\mathbf{u}) \cdot \mathbf{n}$. Such schemes use necessarily entropy stable numerical fluxes as stated below.

LEMMA 3. *Let a three-point numerical scheme of the form (3.6) for the discretization of (2.1) that satisfies the discrete entropy inequality (3.7) with consistent numerical fluxes. Then, the numerical flux in (3.6) is entropy stable in the sense (3.2).*

Proof. Let \mathbf{u}^- and \mathbf{u}^+ in Ω^a and first substitute $\mathbf{U}_{j-1}^n = \mathbf{U}_j^n = \mathbf{u}^-$ and $\mathbf{U}_{j+1}^n = \mathbf{u}^+$ into (3.6) and (3.7), we get $\mathbf{U}_j^{n+1} = \mathbf{u}^- - \frac{\Delta t}{\Delta x} (\mathbf{h}(\mathbf{u}^-, \mathbf{u}^+, \mathbf{n}) - \mathbf{f}(\mathbf{u}^-) \cdot \mathbf{n})$ by consistency of \mathbf{h} so (3.7) becomes

$$\eta\left(\mathbf{u}^- - \frac{\Delta t}{\Delta x} (\mathbf{h}(\mathbf{u}^-, \mathbf{u}^+, \mathbf{n}) - \mathbf{f}(\mathbf{u}^-) \cdot \mathbf{n})\right) - \eta(\mathbf{u}^-) + \frac{\Delta t}{\Delta x} (Q(\mathbf{u}^-, \mathbf{u}^+, \mathbf{n}) - \mathbf{q}(\mathbf{u}^-) \cdot \mathbf{n}) \leq 0,$$

and letting $\Delta t \downarrow 0$ we obtain

$$(\mathbf{f}(\mathbf{u}^-) \cdot \mathbf{n} - \mathbf{h}(\mathbf{u}^-, \mathbf{u}^+, \mathbf{n})) \cdot \boldsymbol{\eta}'(\mathbf{u}^-) + Q(\mathbf{u}^-, \mathbf{u}^+, \mathbf{n}) - \mathbf{q}(\mathbf{u}^-) \cdot \mathbf{n} \leq 0.$$

Now, substituting $\mathbf{U}_{j-1}^n = \mathbf{u}^-$ and $\mathbf{U}_j^n = \mathbf{U}_{j+1}^n = \mathbf{u}^+$ into (3.6) and (3.7) and using the same procedure, we obtain

$$(\mathbf{h}(\mathbf{u}^-, \mathbf{u}^+, \mathbf{n}) - \mathbf{f}(\mathbf{u}^+) \cdot \mathbf{n}) \cdot \boldsymbol{\eta}'(\mathbf{u}^+) + \mathbf{q}(\mathbf{u}^+) \cdot \mathbf{n} - Q(\mathbf{u}^-, \mathbf{u}^+, \mathbf{n}) \leq 0.$$

Summing the two above equations gives the desired result. \square

We now consider a numerical scheme for quadrangular meshes $\Omega_h \subset \mathbb{R}^2$ using the two-point numerical flux in (3.6):

$$(3.8) \quad \mathbf{U}_\kappa^{n+1} = \mathbf{U}_\kappa^n - \frac{\Delta t}{|\kappa|} \sum_{e \in \partial \kappa} |e| \mathbf{h}(\mathbf{U}_\kappa^n, \mathbf{U}_{\kappa_e^+}^n, \mathbf{n}_e) \quad \forall \kappa \in \Omega_h, n \geq 0,$$

where \mathbf{n}_e is the unit outward normal vector on the edge e in $\partial \kappa$, and κ_e^+ the neighboring cell sharing the interface e (see Figure 1). Each element is shape-regular: the ratio of the radius of the largest inscribed ball to the diameter is bounded by below by a positive constant independent of the mesh. We now state the next two results which are extensions to quadrangles of results from [41].

LEMMA 4. *Let a three-point numerical scheme of the form (3.6) with a consistent and conservative numerical flux for the discretization of (2.1a) that satisfies positivity of the solution, $\mathbf{U}_j^{n \geq 0}$ in*

Ω^a , under the CFL condition in (3.6). Then, the numerical scheme (3.8) on quadrangular meshes with the same numerical flux is positive under the condition

$$(3.9) \quad \Delta t \max_{\kappa \in \Omega_h} \frac{|\partial \kappa|}{|\kappa|} \max_{e \in \partial \kappa} |\lambda(\mathbf{U}_{\kappa^\pm}^n)| \leq \alpha_{max}, \quad |\partial \kappa| := \sum_{e \in \partial \kappa} |e|.$$

Proof. Using $\sum_{e \in \partial \kappa} |e| \mathbf{n}_e = 0$, we rewrite (3.8) under the form

$$\begin{aligned} \mathbf{U}_\kappa^{n+1} &= \mathbf{U}_\kappa^n - \frac{\Delta t}{|\kappa|} \sum_{e \in \partial \kappa} |e| (\mathbf{h}(\mathbf{U}_\kappa^n, \mathbf{U}_{\kappa_e^+}^n, \mathbf{n}_e) - \mathbf{f}(\mathbf{U}_\kappa^n) \cdot \mathbf{n}_e) \\ &\stackrel{(3.3)}{=} \mathbf{U}_\kappa^n - \frac{\Delta t}{|\kappa|} \sum_{e \in \partial \kappa} |e| (\mathbf{h}(\mathbf{U}_\kappa^n, \mathbf{U}_{\kappa_e^+}^n, \mathbf{n}_e) - \mathbf{h}(\mathbf{U}_\kappa^n, \mathbf{U}_\kappa^n, \mathbf{n}_e)) \\ &\stackrel{(3.9)}{=} \sum_{e \in \partial \kappa} \frac{|e|}{|\partial \kappa|} \left(\mathbf{U}_\kappa^n - \frac{\Delta t |\partial \kappa|}{|\kappa|} (\mathbf{h}(\mathbf{U}_\kappa^n, \mathbf{U}_{\kappa_e^+}^n, \mathbf{n}_e) - \mathbf{h}(\mathbf{U}_\kappa^n, \mathbf{U}_\kappa^n, \mathbf{n}_e)) \right), \end{aligned}$$

which is a convex combination of positive three-point schemes (3.6) under the condition (3.9). \square

LEMMA 5. Under the assumptions of Lemma 4, the numerical scheme

$$(3.10) \quad \mathbf{U}_\kappa^{n+1} = \mathbf{U}_\kappa^n - \frac{\Delta t}{|\kappa|} \sum_{e \in \partial \kappa} |e| \mathbf{h}(\mathbf{U}_{\kappa_e^-}^n, \mathbf{U}_{\kappa_e^+}^n, \mathbf{n}_e), \quad \sum_{e \in \partial \kappa} \frac{|e|}{|\partial \kappa|} \mathbf{U}_{\kappa_e^-}^n = \mathbf{U}_\kappa^n,$$

on quadrangular meshes is positive under the condition

$$(3.11) \quad \Delta t \max_{\kappa \in \Omega_h} \frac{|\partial \kappa|}{|\kappa|} \max_{e \in \partial \kappa} \frac{|\partial \kappa_e|}{|e|} \max_{f \in \partial \kappa} |\lambda(\mathbf{U}_{\kappa_f^\pm}^n)| \leq \alpha_{max},$$

with $\kappa = \cup_{e \in \partial \kappa} \kappa_e$ divided into sub-triangles as in Figure 1.

Proof. We use the notations in Figure 1. By conservation (3.4), $\mathbf{n}_{ef} = -\mathbf{n}_{fe}$, and $l_{ef} = l_{fe}$, we have

$$\sum_{e \in \partial \kappa} \sum_{f \in \partial \kappa_e \setminus \{e\}} l_{ef} \mathbf{h}(\mathbf{U}_{\kappa_e^-}^n, \mathbf{U}_{\kappa_f^-}^n, \mathbf{n}_{ef}) = 0.$$

Adding this quantity to (3.10), we get

$$\begin{aligned} \mathbf{U}_\kappa^{n+1} &\stackrel{(3.10)}{=} \sum_{e \in \partial \kappa} \frac{|e|}{|\partial \kappa|} \mathbf{U}_{\kappa_e^-}^n - \frac{\Delta t}{|\kappa|} \sum_{e \in \partial \kappa} \left(|e| \mathbf{h}(\mathbf{U}_{\kappa_e^-}^n, \mathbf{U}_{\kappa_e^+}^n, \mathbf{n}_e) - \sum_{f \in \partial \kappa_e \setminus \{e\}} l_{ef} \mathbf{h}(\mathbf{U}_{\kappa_e^-}^n, \mathbf{U}_{\kappa_f^-}^n, \mathbf{n}_{ef}) \right) \\ &= \sum_{e \in \partial \kappa} \frac{|e|}{|\partial \kappa|} \left(\mathbf{U}_{\kappa_e^-}^n - \frac{|\partial \kappa|}{|e|} \frac{\Delta t}{|\kappa|} \sum_{f \in \partial \kappa_e} l_{ef} \mathbf{h}(\mathbf{U}_{\kappa_e^-}^n, \hat{\mathbf{U}}_\kappa^{ef,n}, \mathbf{n}_{ef}) \right), \end{aligned}$$

with the conventions $l_{ee} = |e|$, $\mathbf{n}_{ee} = \mathbf{n}_e$, $\hat{\mathbf{U}}_\kappa^{ee,n} = \mathbf{U}_{\kappa_e^+}^n$, and $\hat{\mathbf{U}}_\kappa^{ef,n} = \mathbf{U}_{\kappa_f^-}^n$ for $f \neq e$. The scheme (3.10) is therefore a convex combination of positive schemes of the form (3.8) under (3.11). \square

4. Relaxation-based numerical flux for the HRM model. The main objective is here the derivation in Theorem 8 of an entropy stable numerical flux for (2.1a). We extend the energy relaxation approximation for the Euler system to the HRM system. The results from [17] do not apply directly because the entropy for the relaxation system is not strictly convex and we circumvent this difficulty in Theorem 7 by introducing another relaxation approximation containing only LD fields [4] together with a variational principle on the entropy.

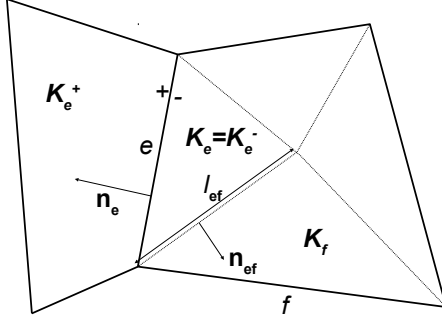


FIG. 1. Quadrangle element κ divided into sub-triangles $\kappa = \cup_{e \in \partial\kappa} \kappa_e$ and notations.

4.1. Energy relaxation system. Following the energy relaxation method introduced in [17], we consider the system

$$(4.1) \quad \partial_t \mathbf{w}^\epsilon + \nabla \cdot \mathbf{g}(\mathbf{w}^\epsilon) = -\frac{1}{\epsilon} (\mathbf{w}^\epsilon - \mathcal{M}(\mathbf{w}^\epsilon)),$$

where

$$(4.2) \quad \mathbf{w} = \begin{pmatrix} \rho Y \\ \rho \\ \rho \mathbf{v} \\ \rho E_r \\ \rho e_s \end{pmatrix}, \quad \mathbf{g}(\mathbf{w}) = \begin{pmatrix} \rho Y \mathbf{v}^\top \\ \rho \mathbf{v}^\top \\ \rho \mathbf{v} \mathbf{v}^\top + p_r(\rho, e_r) \mathbf{I} \\ (\rho E_r + p_r(\rho, e_r)) \mathbf{v}^\top \\ \rho e_s \mathbf{v}^\top \end{pmatrix}, \quad \mathbf{w} - \mathcal{M}(\mathbf{w}) = \begin{pmatrix} 0 \\ 0 \\ 0 \\ 0 \\ -\rho(e_s - F(Y, e_r)) \\ \rho(e_s - F(Y, e_r)) \end{pmatrix},$$

with $\epsilon > 0$ the relaxation time scale, $e_r = E_r - \frac{\mathbf{v} \cdot \mathbf{v}}{2}$, and

$$(4.3) \quad p_r(\rho, e_r) = (\gamma - 1)\rho e_r,$$

where γ is defined by

$$(4.4) \quad \gamma > \max_{0 \leq Y \leq 1} \gamma(Y) \stackrel{(2.12)}{=} \gamma_1 > 1.$$

and constitutes the subcharacteristic condition for (4.1) to relax to an equilibrium as $\epsilon \downarrow 0$ [17]. Let $\mathbf{w} = \lim_{\epsilon \downarrow 0} \mathbf{w}^\epsilon$, in this limit, one formally recovers (2.1a) with

$$(4.5) \quad \mathbf{w} = \mathcal{M}(\mathbf{w}), \quad \mathbf{u} = \mathcal{L}\mathbf{w} := (w_1, \dots, w_{d+2}, w_{d+3} + w_{d+4})^\top, \quad \mathbf{f}(\mathbf{u}) = \mathcal{L}\mathbf{g}(\mathcal{P}(\mathbf{u})),$$

and the prolongation operator $\mathcal{P} : \Omega^a \ni \mathbf{u} \mapsto \mathcal{P}(\mathbf{u}) = (\rho Y, \rho, \rho \mathbf{v}, \rho e_r(\rho, \mathbf{p}) + \rho \frac{\mathbf{v} \cdot \mathbf{v}}{2}, \rho(e - e_r(\rho, \mathbf{p})))^\top$ in Ω^r with $e_r(\rho, \mathbf{p}_r)$ defined from (4.3) and $\mathbf{p} = \mathbf{p}(Y, \rho, e)$ defined from (2.6). The set of states for (4.1) is $\Omega^r = \{\mathbf{w} \in \mathbb{R}^{d+4} : 0 \leq Y \leq 1, \rho > 0, e_r > 0, e_s > 0\}$. The equilibrium (4.5) corresponds to

$$(4.6) \quad E = E_r + e_s, \quad e = e_r + e_s, \quad e_s = F(Y, e_r) := \frac{\gamma - \gamma(Y)}{\gamma(Y) - 1} e_r,$$

where the expression for F follows from the consistency relation on the pressure and (2.6b): $p(Y, \rho, e_r + F(Y, e_r)) = p_r(\rho, e_r)$. Note that (4.1) admits an entropy inequality for the following convex entropy associated with (4.3) [17]:

$$(4.7) \quad s_r(\rho, e_r) = -\left(\frac{e_r}{\rho^{\gamma-1}}\right)^{\frac{1}{\gamma}}.$$

Now, let $\tau = \frac{1}{\rho}$ be the covolume and introduce the following functions

$$(4.8a) \quad \zeta(Y, \tau, e_r, e_s) = -s\left(Y, \mathcal{R}\left(Y, s_r\left(\frac{1}{\tau}, e_r\right), e_s\right), \mathcal{E}(Y, e_s) + e_s\right),$$

$$(4.8b) \quad \mathcal{E}(Y, e_s) = \frac{\gamma(Y)-1}{\gamma-\gamma(Y)} e_s, \quad \mathcal{R}(Y, s_r, e_s) = \left(\frac{1}{(-s_r)^\gamma} \frac{\gamma(Y)-1}{\gamma-\gamma(Y)} e_s\right)^{\frac{1}{\gamma-1}},$$

where s is the mixture entropy (2.16) for the HRM system, the function \mathcal{E} solves $e_s = F(Y, e_r)$ for e_r with F defined in (4.6), while \mathcal{R} solves $s_r = s_r(\rho, \mathcal{E}(Y, e_s))$ for ρ through (4.7). Using (2.16) and (4.8), we easily obtain

$$(4.9a) \quad \zeta(Y, \tau, e_r, e_s) = -s\left(Y, \frac{1}{\tau}, e_r + e_s\right) + \varsigma(Y, e_r, e_s),$$

$$(4.9b) \quad \varsigma(Y, e_r, e_s) = C_v(Y) \ln \left(\frac{\gamma-\gamma(Y)}{\gamma-1} \frac{e_r+e_s}{e_s} \left(\frac{\gamma(Y)-1}{\gamma-\gamma(Y)} \frac{e_s}{e_r} \right)^{\frac{\gamma(Y)-1}{\gamma-1}} \right).$$

We now prove the following variational principle.

LEMMA 6. *Under the assumption (4.4), the function $\rho\zeta$ defined by (4.8) is a (non strictly) convex entropy for (4.1) that satisfies the following variational principle:*

$$(4.10) \quad -s(Y, \rho, e) = \min_{e_r+e_s=e} \{\zeta(Y, \frac{1}{\rho}, e_r, e_s) : 0 \leq Y \leq 1, \rho > 0, e_r > 0, e_s > 0\}.$$

Proof. First, from (4.8a), one may rewrite $\zeta(Y, \tau, e_r, e_s) = \Sigma(Y, s_r(\frac{1}{\tau}, e_r), e_s)$, and for smooth solutions of (4.1), we have

$$(4.11) \quad \partial_t \rho^\epsilon \Sigma(Y^\epsilon, s_r^\epsilon, e_s^\epsilon) + \nabla \cdot (\rho^\epsilon \Sigma(Y^\epsilon, s_r^\epsilon, e_s^\epsilon) \mathbf{v}^\epsilon) = \frac{1}{\epsilon} \rho^\epsilon (\partial_{s_r} \Sigma \partial_{e_r} s_r - \partial_{e_s} \Sigma)^\epsilon (e_s^\epsilon - F(Y^\epsilon, e_r^\epsilon)).$$

Now we observe that from (4.3) $\rho^\epsilon Y^\epsilon$ is uncoupled from other variables in (4.1), thus Y acts only as a frozen parameter in the definitions (4.6) and (4.8). The pressure laws (2.6b) and (4.3) with (4.4) thus satisfy the assumptions of Theorem 2.1 in [17], so the RHS of (4.11) is negative. To prove that $\rho\zeta(\mathbf{w})$ is convex it is sufficient to prove that $\zeta(Y, \tau, e_r, e_s)$ is convex [25, chap. 2]. Using algebraic manipulations that are left to the reader, the Hessian of ζ reads

$$\mathcal{H}_\zeta(Y, \tau, e_r, e_s) = \begin{pmatrix} \frac{\gamma'(Y)^2 C_v(Y)}{(\gamma-\gamma(Y))(\gamma(Y)-1)} + \frac{C_v'(Y)^2}{C_v(Y)} + \frac{r'(Y)^2}{r(Y)} & -\frac{r'(Y)}{\tau} & -\frac{r'(Y)}{(\gamma-1)e_r} & \frac{r'(Y)-(\gamma-1)C_v'(Y)}{(\gamma-1)e_s} \\ -\frac{r'(Y)}{\tau} & \frac{r(Y)}{\tau^2} & 0 & 0 \\ -\frac{r'(Y)}{(\gamma-1)e_r} & 0 & \frac{r(Y)}{(\gamma-1)e_r^2} & 0 \\ \frac{r'(Y)-(\gamma-1)C_v'(Y)}{(\gamma-1)e_s} & 0 & 0 & \frac{C_v(Y)}{e_s^2} \left(1 - \frac{\gamma(Y)-1}{\gamma-1}\right) \end{pmatrix}$$

and it may be easily checked that the principal minors are all positive under the condition (4.4) and that the determinant vanishes.

Then, we need to prove that ς in (4.9) is positive and vanishes at equilibrium (4.6) that constitutes a global minimum. Let us rewrite ς as $C_v(Y) \ln(f(\alpha, x))$ with $f(\alpha, x) = \frac{(1-\alpha)(1+x)}{x} \left(\frac{\alpha x}{1-\alpha}\right)^\alpha$,

$x = \frac{e_s}{e_r} > 0$, and $\alpha = \frac{\gamma(Y)-1}{\gamma-1}$ in $(0, 1)$ from (4.4). We have $\partial_x f(\alpha, x) = \frac{1-\alpha}{x^2}(\alpha x + \alpha - 1)$, thus $\partial_x f(\alpha, x) < 0$ for $0 < x < x_{min} := \frac{1-\alpha}{\alpha}$, $\partial_x f(\alpha, x) > 0$ for $x > x_{min}$, and $\partial_x f(\alpha, x_{min}) = 0$. Since $f(\alpha, x_{min}) = 1$, ς vanishes at the global minimum $\alpha x_{min} = 1 - \alpha \Leftrightarrow \frac{\gamma(Y)-1}{\gamma-1} \frac{e_s}{e_r} = 1 - \frac{\gamma(Y)-1}{\gamma-1}$ which indeed corresponds to the equilibrium (4.6): $e_s = F(Y, e_r)$. \square

4.2. Entropy stability through relaxation. The interest in considering the relaxation system (4.1) is that it is possible to derive an entropy stable and consistent numerical flux for (2.1a) from another relaxation based entropy stable and consistent numerical flux for (4.1). One of these numerical fluxes is the approximate Riemann solver from [4, Prop. 2.21] based on pressure relaxation and introduced in subsection 4.3. The associated numerical scheme reads

$$(4.12) \quad \mathbf{W}_j^{n+1} - \mathbf{W}_j^n + \frac{\Delta t}{\Delta x} (\mathbf{H}(\mathbf{W}_j^n, \mathbf{W}_{j+1}^n, \mathbf{n}) - \mathbf{H}(\mathbf{W}_{j-1}^n, \mathbf{W}_j^n, \mathbf{n})) = 0,$$

with $\mathbf{H}(\mathbf{w}, \mathbf{w}, \mathbf{n}) = \mathbf{g}(\mathbf{w}) \cdot \mathbf{n}$. The numerical flux $\mathbf{H}(\cdot, \cdot, \cdot)$ solves the exact Riemann problem for the pressure relaxation system [4, Sec. 2.4.6] containing only LD fields and, under the CFL condition (4.18), we have

$$(4.13) \quad \rho\zeta(\mathbf{W}_j^{n+1}) \leq \langle \rho\zeta(\mathcal{W}_h^{n+1}) \rangle_j = \rho\zeta(\mathbf{W}_j^n) - \frac{\Delta t}{\Delta x} (Z(\mathbf{W}_j^n, \mathbf{W}_{j+1}^n, \mathbf{n}) - Z(\mathbf{W}_{j-1}^n, \mathbf{W}_j^n, \mathbf{n})),$$

with $Z(\mathbf{w}, \mathbf{w}, \mathbf{n}) = \rho\zeta\mathbf{v} \cdot \mathbf{n}$, $\langle \cdot \rangle_j$ the cell average, and $\mathcal{W}_h^{n+1}(\cdot)$ is the exact solution resulting from local Riemann problems at mesh interfaces of the pressure based relaxation system [4, Sec. 2.4.6] associated to $\mathbf{W}_{j \in \mathbb{Z}}^n$ as initial condition (with some slight abuse). The equality in (4.13) results from the fact that the pressure relaxation system contains only LD fields and [25, Th. 5.3], while the inequality follows from relaxation, then cell-averaging the exact solution via a Jensen's inequality.

THEOREM 7. *Consider the three-point numerical scheme (4.12) for (4.1) satisfying (4.13) with consistent numerical fluxes. Then, the three-point numerical scheme (3.6) with the consistent numerical flux $\mathbf{h}(\mathbf{u}^-, \mathbf{u}^+, \mathbf{n}) = \mathcal{L}\mathbf{H}(\mathcal{P}(\mathbf{u}^-), \mathcal{P}(\mathbf{u}^+), \mathbf{n})$ is entropy stable for the pair (η, \mathbf{q}) in (2.13) and satisfies (3.7) with $Q(\mathbf{u}^-, \mathbf{u}^+, \mathbf{n}) = Z(\mathcal{P}(\mathbf{u}^-), \mathcal{P}(\mathbf{u}^+), \mathbf{n})$.*

Proof. By consistency of \mathbf{H} : $\mathbf{h}(\mathbf{u}, \mathbf{u}, \mathbf{n}) = \mathcal{L}\mathbf{H}(\mathcal{P}(\mathbf{u}), \mathcal{P}(\mathbf{u}), \mathbf{n}) = \mathcal{L}\mathbf{g}(\mathcal{P}(\mathbf{u})) \cdot \mathbf{n} \stackrel{(4.5)}{=} \mathbf{f}(\mathbf{u}) \cdot \mathbf{n}$. Then, let $\mathbf{W}_j^n = \mathcal{P}(\mathbf{U}_j^n)$ so $\rho\zeta(\mathbf{W}_j^n) = \eta(\mathbf{U}_j^n)$ and $Z(\mathbf{W}_j^n, \mathbf{W}_{j+1}^n, \mathbf{n}) = Q(\mathbf{U}_j^n, \mathbf{U}_{j+1}^n, \mathbf{n})$, and define \mathbf{W}_j^{n+1} from (4.12) and $\mathbf{U}_j^{n+1} = \mathcal{L}\mathbf{W}_j^{n+1}$. By the variational principle (4.10) and Jensen's inequality:

$$\langle \rho\zeta(\mathcal{W}_h^{n+1}) \rangle_j \stackrel{(4.10)}{\geq} \langle \eta(\mathcal{L}\mathcal{W}_h^{n+1}) \rangle_j \geq \eta(\langle \mathcal{L}\mathcal{W}_h^{n+1} \rangle_j) = \eta(\mathbf{U}_j^{n+1}),$$

from which we deduce

$$\begin{aligned} \eta(\mathbf{U}_j^{n+1}) &\stackrel{(4.13)}{\leq} \rho\zeta(\mathbf{W}_j^n) - \frac{\Delta t}{\Delta x} (Z(\mathbf{W}_j^n, \mathbf{W}_{j+1}^n, \mathbf{n}) - Z(\mathbf{W}_{j-1}^n, \mathbf{W}_j^n, \mathbf{n})) \\ &= \rho\zeta(\mathcal{P}(\mathbf{U}_j^n)) - \frac{\Delta t}{\Delta x} (Z(\mathcal{P}(\mathbf{U}_j^n), \mathcal{P}(\mathbf{U}_{j+1}^n), \mathbf{n}) - Z(\mathcal{P}(\mathbf{U}_{j-1}^n), \mathcal{P}(\mathbf{U}_j^n), \mathbf{n})) \\ &= \eta(\mathbf{U}_j^n) - \frac{\Delta t}{\Delta x} (Q(\mathbf{U}_j^n, \mathbf{U}_{j+1}^n, \mathbf{n}) - Q(\mathbf{U}_{j-1}^n, \mathbf{U}_j^n, \mathbf{n})), \end{aligned}$$

which concludes the proof. \square

4.3. Entropy stable and positive three-point scheme. We here introduce a numerical flux that leads to an entropy stable three-point scheme for the relaxation system (4.1). Such numerical flux defines an entropy stable scheme for the HRM system (2.1a) as stated in Theorem 8.

Let us consider the following numerical flux based on relaxation of pressure [4, Prop. 2.21]:

$$(4.14) \quad \mathbf{h}(\mathbf{u}^-, \mathbf{u}^+, \mathbf{n}) = \mathbf{f}(\mathcal{W}^r(0; \mathbf{u}^-, \mathbf{u}^+, \mathbf{n})) \cdot \mathbf{n},$$

where the Riemann solver $\mathcal{W}^r(\cdot; \mathbf{u}_L, \mathbf{u}_R, \mathbf{n})$ is used to approximate the solution to (2.1) in the direction \mathbf{n} with initial data, $\mathbf{u}_0(x) = \mathbf{u}_L$ if $x := \mathbf{x} \cdot \mathbf{n} < 0$ and $\mathbf{u}_0(x) = \mathbf{u}_R$ if $\mathbf{x} \cdot \mathbf{n} > 0$, and reads

$$(4.15) \quad \mathcal{W}^r\left(\frac{x}{t}; \mathbf{u}_L, \mathbf{u}_R, \mathbf{n}\right) = \begin{cases} \mathbf{u}_L, & \frac{x}{t} \leq S_L, \\ \mathbf{u}^*, & S_L < \frac{x}{t} < u^*, \\ \mathbf{u}_R^*, & u^* < \frac{x}{t} < S_R, \\ \mathbf{u}_R, & S_R \leq \frac{x}{t}, \end{cases}$$

where $\mathbf{u}_L^* = (\rho_L^* Y_L, \rho_L^*, \rho_L^* \mathbf{v}_L^*, \rho_L^* E_L^*)^\top$, $\mathbf{u}_R^* = (\rho_R^* Y_R, \rho_R^*, \rho_R^* \mathbf{v}_R^*, \rho_R^* E_R^*)^\top$, and

$$(4.16a) \quad \mathbf{v}_L^* = \mathbf{v}_L + (u^* - u_L)\mathbf{n}, \quad \mathbf{v}_R^* = \mathbf{v}_R + (u^* - u_R)\mathbf{n},$$

$$(4.16b) \quad u^* = \frac{a_L u_L + a_R u_R + p_L - p_R}{a_L + a_R}, \quad p^* = \frac{a_R p_L + a_L p_R + a_L a_R (u_L - u_R)}{a_L + a_R},$$

$$(4.16c) \quad \tau_L^* = \tau_L + \frac{u^* - u_L}{a_L}, \quad \tau_R^* = \tau_R + \frac{u_R - u^*}{a_R},$$

$$(4.16d) \quad E_L^* = E_L - \frac{p^* u^* - p_L u_L}{a_L}, \quad E_R^* = E_R - \frac{p_R u_R - p^* u^*}{a_R},$$

where $u_X = \mathbf{v}_X \cdot \mathbf{n}$ and $p_X = p(Y_X, \rho_X, e_X)$ defined by (2.6b) for $X = L, R$; (4.16a) corresponds to a decomposition into normal, u_X , and tangential, $\mathbf{v}_X - u_X \mathbf{n}$, components of the velocity vector.

The wave speeds are evaluated from $S_L = u_L - a_L/\rho_L$ and $S_R = u_R + a_R/\rho_R$ where the approximate Lagrangian sound speeds [4] are defined by

$$(4.17a) \quad \begin{cases} \frac{a_L}{\rho_L} &= c_\gamma(\rho_L, p_L) + \frac{\gamma+1}{2} \left(\frac{p_R - p_L}{\rho_R c_\gamma(\rho_R, p_R)} + u_L - u_R \right)^+, \\ \frac{a_R}{\rho_R} &= c_\gamma(\rho_R, p_R) + \frac{\gamma+1}{2} \left(\frac{p_L - p_R}{a_L} + u_L - u_R \right)^+ \end{cases}, \quad \text{if } p_R \geq p_L,$$

$$(4.17b) \quad \begin{cases} \frac{a_R}{\rho_R} &= c_\gamma(\rho_R, p_R) + \frac{\gamma+1}{2} \left(\frac{p_L - p_R}{\rho_L c_\gamma(\rho_L, p_L)} + u_L - u_R \right)^+, \\ \frac{a_L}{\rho_L} &= c_\gamma(\rho_L, p_L) + \frac{\gamma+1}{2} \left(\frac{p_R - p_L}{a_R} + u_L - u_R \right)^+ \end{cases}, \quad \text{else,}$$

where $(\cdot)^+ = \max(\cdot, 0)$ denotes the positive part and $c_\gamma(\rho, p) = \sqrt{\gamma p / \rho}$ with γ defined by (4.4).

THEOREM 8. *The numerical flux (4.14) for (2.1a) defined by (4.15), (4.16) and (4.17) is entropy stable in the sense (3.2) for the pair (2.14). Moreover, the associated three-point scheme (3.6) preserves the invariant domain (2.10) under the condition*

$$(4.18) \quad \frac{\Delta t}{\Delta x} \max_{j \in \mathbb{Z}} |\lambda(\mathbf{U}_j^n)| < \frac{1}{2}, \quad |\lambda(\mathbf{u})| := |\mathbf{v} \cdot \mathbf{n}| + \frac{a}{\rho}.$$

Proof. By applying [4, Prop. 2.21], one defines from (4.15), (4.16) and (4.17) an entropy stable three-point scheme (4.12) and (4.13) for the relaxation system (4.1) since ρY and ρe_s are only purely advected in (4.1). The associated approximate Riemann solver uses the intermediate states $\mathbf{w}_X^* = (\rho_X^* Y_X, \rho_X^*, \rho_X^* \mathbf{v}_X^*, \rho_X^* E_{r,X}^*, \rho_X^* e_{s,X})^\top$ with $X = L, R$. Condition (4.4) and Theorem 7 ensure

that one deduces a three-point numerical scheme for (2.1a) that is entropy stable for (η, \mathbf{q}) in (2.13) and satisfies (3.7). We then conclude by applying Lemma 3 and (4.14) is obtained by summing the two last components of the numerical flux for (4.1).

Positivity for density and internal energy under (4.18) follows again from [4, Prop. 2.21]. Note that the intermediate states for Y in (4.16) are Y_L and Y_R . The approximate Riemann solver thus preserves the invariant domain for Y , so the three-point scheme since from (4.14) and (4.15) ρY_j^{n+1} is the cell-average of exact solutions to local Riemann problems at interfaces. \square

5. DGSEM formulation. The DG method consists in defining a semi-discrete weak formulation of problem (2.1). The domain is discretized with a shape-regular mesh $\Omega_h \subset \mathbb{R}^d$ consisting of nonoverlapping and nonempty cells κ . By \mathcal{E} we define the set of interfaces in Ω_h . For the sake of clarity, we introduce the DGSEM in two space dimensions $d = 2$, the extension (resp. restriction) to $d = 3$ (resp. $d = 1$) being straightforward.

5.1. Numerical solution. We look for approximate solutions in the function space of discontinuous polynomials $\mathcal{V}_h^p = \{\phi \in L^2(\Omega_h) : \phi|_{\kappa} \circ \mathbf{x}_{\kappa} \in \mathcal{Q}^p(I^2) \forall \kappa \in \Omega_h\}$, where $\mathcal{Q}^p(I^2)$ denotes the space of functions over the master element $I^2 := \{\boldsymbol{\xi} = (\xi, \eta) : -1 \leq \xi, \eta \leq 1\}$, formed by tensor products of polynomials of degree at most p in each direction. Each physical element κ is the image of I^2 through the mapping $\mathbf{x}_{\kappa} = \mathbf{x}_{\kappa}(\boldsymbol{\xi})$. Likewise, each face in \mathcal{E} is the image of $I = [-1, 1]$ through the mapping $\mathbf{x}_e = \mathbf{x}_e(\xi)$. The approximate solution to (2.1) is sought under the form

$$(5.1) \quad \mathbf{u}_h(\mathbf{x}, t) = \sum_{0 \leq i, j \leq p} \phi_{\kappa}^{ij}(\mathbf{x}) \mathbf{U}_{\kappa}^{ij}(t) \quad \forall \mathbf{x} \in \kappa, \kappa \in \Omega_h, \forall t \geq 0,$$

where $(\mathbf{U}_{\kappa}^{ij})_{0 \leq i, j \leq p}$ are the degrees of freedom (DOFs) in the element κ . The subset $(\phi_{\kappa}^{ij})_{0 \leq i, j \leq p}$ constitutes a basis of \mathcal{V}_h^p restricted onto the element κ and $(p+1)^2$ is its dimension.

Let $(\ell_k)_{0 \leq k \leq p}$ be the Lagrange interpolation polynomials in one space dimension associated to the Gauss-Lobatto nodes over I : $\xi_0 = -1 < \xi_1 < \dots < \xi_p = 1$:

$$(5.2) \quad \ell_k(\xi_l) = \delta_{k,l}, \quad 0 \leq k, l \leq p,$$

with $\delta_{k,l}$ the Kronecker symbol. In this work we use tensor products of these polynomials and of Gauss-Lobatto nodes (see Figure 2):

$$(5.3) \quad \phi_{\kappa}^{ij}(\mathbf{x}) = \phi^{ij}(\mathbf{x}_{\kappa}(\boldsymbol{\xi})) = \ell_i(\xi) \ell_j(\eta), \quad 0 \leq i, j \leq p.$$

which satisfy the following relation at quadrature points $\boldsymbol{\xi}_{i'j'} = (\xi_{i'}, \eta_{j'}) \in I^2$:

$$(5.4) \quad \phi_{\kappa}^{ij}(\mathbf{x}_{\kappa}^{i'j'}) = \delta_{i,i'} \delta_{j,j'}, \quad 0 \leq i, j, i', j' \leq p, \quad \mathbf{x}_{\kappa}^{i'j'} := \mathbf{x}_{\kappa}(\boldsymbol{\xi}_{i'j'}),$$

so the DOFs correspond to the point values of the solution: $\mathbf{U}_{\kappa}^{ij}(t) = \mathbf{u}_h(\mathbf{x}_{\kappa}^{ij}, t)$.

Let introduce the discrete derivative matrix of the Lagrange polynomials in I with entries

$$(5.5) \quad D_{kl} = \ell'_l(s_k), \quad 0 \leq k, l \leq p.$$

In the DGSEM, the integrals over elements and faces are approximated by using the Gauss-Lobatto quadrature rule so the quadrature and interpolation nodes are collocated:

$$(5.6) \quad \int_{\kappa} f(\mathbf{x}) dV \simeq \sum_{0 \leq i, j \leq p} \omega_i \omega_j J_{\kappa}^{ij} f(\mathbf{x}_{\kappa}^{ij}), \quad \int_e f(\mathbf{x}) dS \simeq \sum_{0 \leq k \leq p} \omega_k \frac{|e|}{2} f(\mathbf{x}_e^k),$$

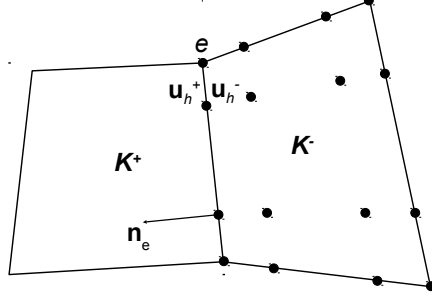


FIG. 2. Inner and outer elements, κ^- and κ^+ , for $d = 2$; definitions of traces \mathbf{u}_h^\pm on the interface e and of the unit outward normal vector \mathbf{n}_e ; positions of quadrature points in κ^- and on e for $p = 3$.

with $\omega_l > 0$ and \mathbf{x}_κ^{ij} the weights and nodes of the quadrature rule, and $J_\kappa^{ij} = \det(\partial_\xi \mathbf{x}_\kappa(\xi_{ij})) > 0$.

Note that we will use cell-averaged quantities, for instance for the numerical solution

$$(5.7) \quad \frac{1}{|\kappa|} \int_\kappa \mathbf{u}_h(\mathbf{x}, t) dV \simeq \langle \mathbf{u}_h \rangle_\kappa(t) := \sum_{1 \leq i, j \leq p} \omega_i \omega_j \frac{J_\kappa^{ij}}{|\kappa|} \mathbf{U}_\kappa^{ij}(t),$$

where $|\kappa|$ is evaluated through numerical quadrature so the weights satisfy

$$(5.8) \quad \sum_{1 \leq i, j \leq p} \omega_i \omega_j \frac{J_\kappa^{ij}}{|\kappa|} = 1.$$

5.2. Space discretization. The semi-discrete form of the DGSEM in space of problem (2.1) starts from the following problem: find \mathbf{u}_h in $(\mathcal{V}_h^p)^{d+3}$ such that

$$(5.9) \quad \int_{\Omega_h} v_h \partial_t \mathbf{u}_h dV + \sum_{\kappa \in \Omega_h} \int_\kappa v_h \nabla \cdot \mathbf{f}(\mathbf{u}_h) dV - \int_{\mathcal{E}} \llbracket v_h \rrbracket \mathbf{h}(\mathbf{u}_h^-, \mathbf{u}_h^+, \mathbf{n}) - \llbracket v_h \mathbf{f}(\mathbf{u}_h) \rrbracket \cdot \mathbf{n} dS = 0 \quad \forall v_h \in \mathcal{V}_h^p, t > 0,$$

where $\llbracket v_h \rrbracket = v_h^+ - v_h^-$ denotes the jump operator and $v_h^\pm(\mathbf{x}) = \lim_{\epsilon \downarrow 0} v_h(\mathbf{x} \pm \epsilon \mathbf{n})$ are the traces of v_h at a point \mathbf{x} on \mathcal{E} and \mathbf{n} denotes the unit normal vector to an interface e in \mathcal{E} . The entropy stable relaxation-based numerical flux (4.14) is used to define $\mathbf{h}(\cdot, \cdot, \cdot)$. Substituting v_h for the Lagrange interpolation polynomials (5.3) and using the Gauss-Lobatto quadrature rules (5.6) to approximate the volume and surface integrals, (5.9) becomes: for all $\kappa \in \Omega_h$, $0 \leq i, j \leq p$, and $t > 0$, we have

$$\begin{aligned} \omega_i \omega_j J_\kappa^{ij} \frac{d\mathbf{U}_\kappa^{ij}}{dt} + \omega_i \omega_j J_\kappa^{ij} \left(\sum_{k=0}^p D_{ik} \mathbf{f}(\mathbf{U}_\kappa^{kj}) \nabla \xi(\xi_{ij}) + \sum_{k=0}^p D_{jk} \mathbf{f}(\mathbf{U}_\kappa^{ik}) \nabla \eta(\xi_{ij}) \right) \\ + \omega_i \left(J_e^{ip} \delta_{jp} \mathbf{d}(\mathbf{x}_\kappa^{ip}, t) + J_e^{i0} \delta_{j0} \mathbf{d}(\mathbf{x}_\kappa^{i0}, t) \right) + \omega_j \left(J_e^{pj} \delta_{ip} \mathbf{d}(\mathbf{x}_\kappa^{pj}, t) + J_e^{0j} \delta_{i0} \mathbf{d}(\mathbf{x}_\kappa^{0j}, t) \right) = 0, \end{aligned}$$

where $\mathbf{d}(\mathbf{x}, t) = \mathbf{h}(\mathbf{u}_h^-(\mathbf{x}, t), \mathbf{u}_h^+(\mathbf{x}, t), \mathbf{n}_e(\mathbf{x})) - \mathbf{f}(\mathbf{u}_h^-(\mathbf{x}, t)) \cdot \mathbf{n}_e(\mathbf{x})$ denotes the numerical flux in fluctuation form at point \mathbf{x} on an interface e , \mathbf{n}_e is the unit outward normal vector at e , $\mathbf{u}_h^\pm(\mathbf{x}, t)$

denote the traces of the numerical solution on e (see Figure 2), and $J_e^{ip} := \det(\partial_\xi \mathbf{x}_e)_{\mathbf{x}_\kappa^{ip}}$ where \mathbf{x}_κ^{ip} , $0 \leq i \leq p$, uniquely identify e .

As explained in the introduction, the volume integral in the above equation is modified so as to satisfy an entropy balance [8, 54]. The semi-discrete entropy stable scheme thus reads

$$(5.10) \quad \omega_i \omega_j J_\kappa^{ij} \frac{d\mathbf{U}_\kappa^{ij}}{dt} + \mathbf{R}_\kappa^{ij}(\mathbf{u}_h) = 0 \quad \forall \kappa \in \Omega_h, \quad 0 \leq i, j \leq p, \quad t > 0,$$

with

$$(5.11) \quad \begin{aligned} \mathbf{R}_\kappa^{ij}(\mathbf{u}_h) = & 2\omega_i \omega_j \left(\sum_{k=0}^p D_{ik} \mathbf{h}_{ec}(\mathbf{U}_\kappa^{ij}, \mathbf{U}_\kappa^{kj}, \{J_\kappa \nabla \xi\}_{(i,k)j}) + \sum_{k=0}^p D_{jk} \mathbf{h}_{ec}(\mathbf{U}_\kappa^{ij}, \mathbf{U}_\kappa^{ik}, \{J_\kappa \nabla \eta\}_{i(j,k)}) \right) \\ & + \omega_i \left(J_e^{ip} \delta_{jp} \mathbf{d}(\mathbf{x}_\kappa^{ip}, t) + J_e^{i0} \delta_{j0} \mathbf{d}(\mathbf{x}_\kappa^{i0}, t) \right) + \omega_j \left(J_e^{pj} \delta_{ip} \mathbf{d}(\mathbf{x}_\kappa^{pj}, t) + J_e^{0j} \delta_{i0} \mathbf{d}(\mathbf{x}_\kappa^{0j}, t) \right), \end{aligned}$$

where $\{J_\kappa \nabla \xi\}_{(i,k)j} = \frac{1}{2}(J_\kappa^{ij} \nabla \xi(\boldsymbol{\xi}_{ij}) + J_\kappa^{kj} \nabla \xi(\boldsymbol{\xi}_{kj}))$, $\{J_\kappa \nabla \eta\}_{i(j,k)} = \frac{1}{2}(J_\kappa^{ij} \nabla \eta(\boldsymbol{\xi}_{ij}) + J_\kappa^{ik} \nabla \eta(\boldsymbol{\xi}_{ik}))$, and $\mathbf{h}_{ec}(\cdot, \cdot, \cdot)$ denotes the entropy conservative numerical flux (3.5).

The works in [8, 24, 54] showed that (5.10) is conservative, high-order accurate and satisfies the semi-discrete entropy inequality for the cell-averaged entropy $\langle \eta(\mathbf{u}_h) \rangle_\kappa$:

$$(5.12) \quad |\kappa| \frac{d\langle \eta(\mathbf{u}_h) \rangle_\kappa}{dt} + \sum_{e \in \partial \kappa} \sum_{k=0}^p \omega_k J_e(\mathbf{x}_e^k) Q(\mathbf{u}_h^-(\mathbf{x}_e^k, t), \mathbf{u}_h^+(\mathbf{x}_e^k, t), \mathbf{n}_e) \leq 0,$$

where $Q(\cdot, \cdot, \cdot)$ denotes the numerical flux in (3.7).

6. Fully discrete scheme. We now focus on the fully discrete scheme and we first use a one-step first-order explicit time discretization and analyze its properties. High-order time integration will be done by using strong-stability preserving explicit Runge-Kutta methods [50] that keeps the properties of the first-order in time scheme under some condition on the time step. We restrict the present analysis to meshes with straight-sided cells.

6.1. Time discretization. Let $t^{(n)} = n\Delta t$, with $\Delta t > 0$ the time step, and use the notations $\mathbf{u}_h^{(n)}(\cdot) = \mathbf{u}_h(\cdot, t^{(n)})$ and $\mathbf{U}_\kappa^{ij,n} = \mathbf{U}_\kappa^{ij}(t^{(n)})$. The fully discrete DGSEM scheme for (2.1) reads

$$(6.1) \quad J_\kappa^{ij} \omega_i \omega_j \frac{\mathbf{U}_\kappa^{ij,n+1} - \mathbf{U}_\kappa^{ij,n}}{\Delta t} + \mathbf{R}_\kappa^{ij}(\mathbf{u}_h^{(n)}) = 0 \quad \forall \kappa \in \Omega_h, \quad 0 \leq i, j \leq p, \quad n \geq 0,$$

where the vector of residuals $\mathbf{R}_\kappa^{ij}(\cdot)$ is defined by (5.11). The projection of the initial condition (2.1b) onto the function space reads $\mathbf{U}_\kappa^{ij,0} = \mathbf{u}_0(\mathbf{x}_\kappa^{ij})$ for all κ in Ω_h and $0 \leq i, j \leq p$.

6.2. Properties of the discrete scheme. We have the following results for the fully discrete solution of the DGSEM that guaranty its positivity and the sharp resolution of contacts in the sense of [27, 17]. Note that we have $J_e \equiv \frac{|e|}{2}$ for straight-sided elements.

THEOREM 9. *Let $n \geq 0$ and assume that $\mathbf{U}_\kappa^{ij,n}$ is in Ω^a for all $0 \leq i, j \leq p$ and κ in Ω_h , then under the CFL condition*

$$(6.2) \quad \Delta t \max_{\kappa \in \Omega_h} \max_{e \in \mathcal{E}} \frac{|\partial \kappa_e|}{|e|} \max_{0 \leq k \leq p} \frac{|\partial \kappa|}{J_\kappa^k} \left| \lambda(\mathbf{u}_h^\pm(\mathbf{x}_e^k, t^{(n)})) \right| < \frac{1}{2p(p+1)},$$

where $\tilde{J}_\kappa^k := \min_{e \in \partial\kappa} J_\kappa(\mathbf{x}_e^k)$, $|\lambda(\cdot)|$ is defined in (4.18) and $\kappa = \cup_{e \in \partial\kappa} \kappa_e$ in Lemma 5, we have

$$(6.3) \quad \langle \mathbf{u}_h^{(n+1)} \rangle_\kappa \in \Omega^a \quad \forall \kappa \in \Omega_h.$$

Moreover, the scheme exactly resolves stationary contact discontinuities at interpolation points.

Proof. The positivity of the solution at time $t^{(n+1)}$ relies on techniques introduced in [41, 57] to rewrite a conservative high-order scheme for the cell-averaged solution as a convex combination of positive quantities. First, consider the three-point scheme (3.6) with the relaxation-based entropy stable numerical flux (4.14). We know by Theorem 8 that this scheme preserves the invariant domain (2.10) under the CFL condition (4.18). The finite volume scheme (3.10) on quadrangles will thus be also positive under the condition (3.11) where $|\lambda(\cdot)|$ is defined in (4.18) and $\alpha_{max} = \frac{1}{2}$.

Now summing (6.1) over $0 \leq i, j \leq p$ gives for the cell-averaged solution

$$\begin{aligned} \langle \mathbf{u}_h^{(n+1)} \rangle_\kappa &\stackrel{(6.1)}{=} \langle \mathbf{u}_h^{(n)} \rangle_\kappa - \frac{\Delta t}{|\kappa|} \sum_{0 \leq i, j \leq p} \mathbf{R}_\kappa^{ij}(\mathbf{u}_h^{(n)}) \\ &\stackrel{(5.11)}{=} \langle \mathbf{u}_h^{(n)} \rangle_\kappa - \frac{\Delta t}{|\kappa|} \sum_{e \in \partial\kappa} \sum_{k=0}^p \omega_k \frac{|e|}{2} \mathbf{h}(\mathbf{u}_h^-(\mathbf{x}_e^k, t^{(n)}), \mathbf{u}_h^+(\mathbf{x}_e^k, t^{(n)}), \mathbf{n}_e). \end{aligned}$$

Using (5.7), $\sum_{e \in \partial\kappa} \frac{|e|}{|\partial\kappa|} = 1$, and $\omega_0 = \omega_p = \frac{2}{p(p+1)}$, we rewrite the above relation as

$$\begin{aligned} \langle \mathbf{u}_h^{(n+1)} \rangle_\kappa &= \sum_{e \in \partial\kappa} \frac{|e|}{|\partial\kappa|} \sum_{0 \leq i, j \leq p} \omega_i \omega_j \frac{J_\kappa^{ij}}{|\kappa|} \mathbf{U}_\kappa^{ij, n} - \frac{\Delta t}{|\kappa|} \sum_{e \in \partial\kappa} \sum_{k=0}^p \omega_k \frac{|e|}{2} \mathbf{h}(\mathbf{u}_h^-(\mathbf{x}_e^k, t^{(n)}), \mathbf{u}_h^+(\mathbf{x}_e^k, t^{(n)}), \mathbf{n}_e) \\ &= \sum_{e \in \partial\kappa} \sum_{0 \leq i, j \leq p} \frac{|e|}{|\partial\kappa|} \omega_i \omega_j \frac{J_\kappa^{ij}}{|\kappa|} \mathbf{U}_\kappa^{ij, n} - \sum_{e \in \partial\kappa} \sum_{k=0}^p \frac{|e|}{|\partial\kappa|} \omega_k \omega_0 \frac{\tilde{J}_\kappa^k}{|\kappa|} \mathbf{u}_h^-(\mathbf{x}_e^k, t^{(n)}) \\ &\quad + \sum_{k=0}^p \omega_k \omega_0 \frac{\tilde{J}_\kappa^k}{|\kappa|} \left(\sum_{e \in \partial\kappa} \frac{|e|}{|\partial\kappa|} \mathbf{u}_h^-(\mathbf{x}_e^k, t^{(n)}) - \frac{\Delta t}{2\omega_0 \tilde{J}_\kappa^k} \sum_{e \in \partial\kappa} |e| \mathbf{h}(\mathbf{u}_h^-(\mathbf{x}_e^k, t^{(n)}), \mathbf{u}_h^+(\mathbf{x}_e^k, t^{(n)}), \mathbf{n}_e) \right), \\ &= \sum_{e \in \partial\kappa} \sum_{0 \leq i, j \leq p, \mathbf{x}_\kappa^{ij} \notin e} \frac{|e|}{|\partial\kappa|} \frac{\omega_i \omega_j J_\kappa^{ij}}{|\kappa|} \mathbf{U}_\kappa^{ij, n} + \sum_{e \in \partial\kappa} \sum_{k=0}^p \frac{|e|}{|\partial\kappa|} \omega_k \omega_0 \frac{J_\kappa(\mathbf{x}_e^k) - \tilde{J}_\kappa^k}{|\kappa|} \mathbf{u}_h^-(\mathbf{x}_e^k, t^{(n)}) \\ &\quad + \sum_{e \in \partial\kappa} \sum_{k=0}^p \frac{|e|}{|\partial\kappa|} \frac{\omega_k \omega_0 \tilde{J}_\kappa^k}{|\kappa|} \left(\sum_{e \in \partial\kappa} \frac{|e| \mathbf{u}_h^-(\mathbf{x}_e^k, t^{(n)})}{|\partial\kappa|} - \frac{\Delta t}{2\omega_0 \tilde{J}_\kappa^k} \sum_{e \in \partial\kappa} |e| \mathbf{h}(\mathbf{u}_h^-(\mathbf{x}_e^k, t^{(n)}), \mathbf{u}_h^+(\mathbf{x}_e^k, t^{(n)}), \mathbf{n}_e) \right), \end{aligned}$$

where we have used the fact that the traces $\mathbf{u}_h^-(\mathbf{x}_e^k)$ correspond to some DOF \mathbf{U}_κ^{ij} that share the edge e (see Figure 2). The terms in brackets correspond to the RHS in (3.10) and are therefore positive under the condition (6.2). We thus conclude that $\langle \mathbf{u}_h^{(n+1)} \rangle_\kappa$ is a convex combination of positive quantities with weights $\frac{|e|}{|\partial\kappa|} \omega_i \omega_j J$ with $J = J_\kappa^{ij}$, \tilde{J}_κ^k , or $J_\kappa(\mathbf{x}_e^k) - \tilde{J}_\kappa^k$.

Finally, assume that the initial condition consists in a stationary contact discontinuity with states $Y_L, \rho_L, \mathbf{v} = 0$, and p in Ω_L and $Y_R, \rho_R, \mathbf{v} = 0$, and p in Ω_R with $\overline{\Omega_L} \cup \overline{\Omega_R} = \overline{\Omega}$, then so do the DOFs. The numerical fluxes (3.5) and (4.14) reduce to $\mathbf{h}_{ec}(\mathbf{u}^-, \mathbf{u}^+, \mathbf{n}) = \mathbf{h}(\mathbf{u}^-, \mathbf{u}^+, \mathbf{n}) = (0, 0, \mathbf{p}\mathbf{n}, 0)^\top$ and we easily obtain from (5.11) that $\mathbf{R}_\kappa^{ij}(\mathbf{u}_h^{(n)}) = 0$ so stationary contacts remain stationary for all times and the DOFs are the exact values. Note that when the discontinuity $\overline{\Omega_L} \cap \overline{\Omega_R}$ corresponds to mesh interfaces, the relaxation based approximate Riemann solver (4.15) provides the exact solution and the contact discontinuity is exactly resolved within cell elements. \square

Remark 10. The factor $\omega_0 = \frac{2}{p(p+1)}$ in (6.2) compared to (3.11) may be compared with the results in [57] obtained on Cartesian meshes. Though conditions (6.2) and (3.11) are not optimal, they are sufficient for our purpose with the assumption of a shape-regular mesh. We refer to [6] and references therein for a review on sharp CFL conditions in the context of finite volume schemes.

6.3. Limiting strategy. The properties in Theorem 9 hold only for the cell-averaged numerical solution at time $t^{(n+1)}$, which is not sufficient for robustness and stability of numerical computations. We use the a posteriori limiter introduced in [57] to extend positivity of the solution at nodal values within elements in order to guaranty robustness of the DGSEM.

Note that the positivity of partial densities (2.9) and hyperbolicity through (2.11) require $Y(r_1 - r_2) > -r_2$, which reduces to $Y > -\frac{r_2}{r_1 - r_2}$ (resp. $Y < \frac{r_2}{r_2 - r_1}$) in the case $r_1 > r_2$ (resp. $r_1 < r_2$). We enforce positivity of nodal values by using the linear limiter

$$(6.4) \quad \tilde{\mathbf{u}}_{\kappa}^{ij,n+1} = \theta_{\kappa}(\mathbf{U}_{\kappa}^{ij,n+1} - \langle \mathbf{u}_h^{(n+1)} \rangle_{\kappa}) + \langle \mathbf{u}_h^{(n+1)} \rangle_{\kappa} \quad \forall 0 \leq i, j \leq p, \quad \kappa \in \Omega_h,$$

with $0 \leq \theta_{\kappa} \leq 1$ defined by $\theta_{\kappa} := \min(\theta_{\kappa}^{\rho}, \theta_{\kappa}^Y, \theta_{\kappa}^e)$ where, in the case $r_1 > r_2$:

$$\begin{aligned} \theta_{\kappa}^{\rho} &= \min\left(\frac{\langle \rho_h^{(n+1)} \rangle_{\kappa} - \varepsilon}{\langle \rho_h^{(n+1)} \rangle_{\kappa} - \rho_{\kappa}^{min}}, 1\right), \quad \rho_{\kappa}^{min} = \min_{0 \leq i, j \leq p} \rho_{\kappa}^{ij,n+1}, \\ \theta_{\kappa}^Y &= \min\left(\frac{\langle \rho Y_h^{(n+1)} \rangle_{\kappa} - \langle \rho_h^{(n+1)} \rangle_{\kappa} \left(\varepsilon - \frac{r_2}{r_1 - r_2}\right)}{\langle \rho Y_h^{(n+1)} \rangle_{\kappa} - \langle \rho_h^{(n+1)} \rangle_{\kappa} Y_{\kappa}^{min}}, 1\right), \quad Y_{\kappa}^{min} = \min_{0 \leq i, j \leq p} \frac{\rho_{\kappa}^{ij,n+1}}{\rho_{\kappa}^{ij,n+1}}, \\ \theta_{\kappa}^e &= \min_{0 \leq i, j \leq p} \left(\theta_{\kappa}^{e,ij} : e(\theta_{\kappa}^{e,ij}(\mathbf{U}_{\kappa}^{ij,n+1} - \langle \mathbf{u}_h^{(n+1)} \rangle_{\kappa}) + \langle \mathbf{u}_h^{(n+1)} \rangle_{\kappa}) \geq \varepsilon \right), \end{aligned}$$

and $\varepsilon = 10^{-10}$ a parameter. In the second case $r_1 < r_2$, θ_{κ}^Y is defined by

$$\theta_{\kappa}^Y = \min\left(\frac{\langle \rho Y_h^{(n+1)} \rangle_{\kappa} - \langle \rho_h^{(n+1)} \rangle_{\kappa} \left(\frac{r_2}{r_2 - r_1} + \varepsilon\right)}{\langle \rho Y_h^{(n+1)} \rangle_{\kappa} - \langle \rho_h^{(n+1)} \rangle_{\kappa} Y_{\kappa}^{max}}, 1\right), \quad Y_{\kappa}^{max} = \max_{0 \leq i, j \leq p} \frac{\rho_{\kappa}^{ij,n+1}}{\rho_{\kappa}^{ij,n+1}}.$$

The present limiter on Y was seen to avoid excessive smearing of material interfaces, while damping spurious oscillations. We also note that the limiter (6.4) strengthens the entropy inequality (2.13) at the discrete level in the sense that $\langle \eta(\tilde{\mathbf{u}}_h^{(n+1)}) \rangle_{\kappa} \leq \langle \eta(\mathbf{u}_h^{(n+1)}) \rangle_{\kappa}$ [14, Lemma 3.1].

7. Numerical experiments. In this section we present numerical experiments, obtained with the CFD code *Aghora* developed at ONERA [45], on problems involving discontinuous solutions in one and two space dimensions in order to illustrate the performance of the DGSEM derived in this work. We use a fourth-order accurate ($p = 3$) scheme in space extended to high-order in time by using the three-stage third-order strong-stability preserving Runge-Kutta method [50], while the limiter (6.4) is applied at the end of each stage.

7.1. One-dimensional shock-tube problems. Let consider Riemann problems associated to the initial condition $\mathbf{u}_0(x) = \mathbf{u}_L$ if $x < x_s$ and \mathbf{u}_R if $x > x_s$ (see Table 1 for details).

We first validate the entropy conservation property of the numerical flux (3.5) in Proposition 1. We thus replace the entropy stable numerical flux \mathbf{h} at interfaces in (5.11) by the entropy conservative flux (3.5). We follow the experimental setup introduced in [3] and choose an initial condition corresponding to problem RP0 in Table 1 resulting in the development of weak shock and contact

TABLE 1
Initial conditions and physical parameters of Riemann problems with $U = (Y, \rho, u, p)^\top$.

test	left state \mathcal{U}_L	right state \mathcal{U}_R	x_s	t	γ_1	C_{v_1}	γ_2	C_{v_2}
RP0	$(\frac{2}{5}, 2, 0, 1)^\top$	$(\frac{3}{5}, \frac{3}{2}, 0, 2)^\top$	0	0.2	1.5	1	1.3	1
RP1	$(\frac{1}{2}, 1, 0, 1)^\top$	$(\frac{1}{2}, \frac{1}{8}, 0, 0.1)^\top$	0	0.2	1.5	1	1.3	1
RP2	$(1, 1.602, 0, 1)^\top$	$(0, 1.122, 0, \frac{1}{10})^\top$	-0.1	3×10^{-4}	$\frac{5}{3}$	3.12	1.4	0.743
RP3	$(\frac{1}{5}, 0.99988, -1.99931, \frac{2}{5})^\top$	$(\frac{1}{2}, 0.99988, 1.99931, \frac{2}{5})^\top$	0	0.15	1.5	1	1.3	1
RP4	$(\frac{1}{10}, 2, 0, 1)^\top$	$(\frac{9}{10}, \frac{1}{2}, 0, 1)^\top$	0	0.2	2.0	2	1.2	1

TABLE 2
Entropy conservation error (7.1) and order of convergence \mathcal{O} obtained for problem RP0 ($h = 1/100$, $p = 3$).

	$e_h(t)$	\mathcal{O}
Δt	$1.44875e-07$	—
$\Delta t/2$	$6.85144e-08$	1.08
$\Delta t/4$	$1.47570e-08$	2.22
$\Delta t/8$	$2.02814e-09$	2.86
$\Delta t/16$	$2.56963e-10$	2.98
$\Delta t/32$	$3.21822e-11$	3.00
$\Delta t/64$	$4.02157e-12$	3.00

waves on a domain of unit length with periodic boundary conditions. As a result of entropy conservation of the space discretization, only the time integration scheme should modify the global entropy budget at the discrete level. We thus evaluate the difference

$$(7.1) \quad e_h(t) := \left| \sum_{\kappa \in \Omega_h} \langle \eta(\mathbf{u}_h) - \eta(\mathbf{u}_0) \rangle_{\kappa}(t) \right|,$$

which quantifies the difference between the discrete entropy at final time and the initial entropy over the domain Ω_h . We observe in Table 2 that the error (7.1) decreases to machine accuracy when refining the time step with third-order of convergence as asymptotic limit corresponding to the theoretical approximation order of the time integration scheme [50]. This validates the entropy conservation property of the numerical flux (3.5).

Results for problems RP1 to RP4 are displayed in Figure 3 where we compare the numerical solution in symbols with the exact solution in lines. Problem RP1 corresponds to the classical Sod problem for the compressible Euler equations since the mass fraction is uniform and corresponds to an equivalent $\gamma(Y) = 1.4$ for the mixture. Problem RP2 comes from [31] and corresponds to a He-N₂ shock tube problem, RP3 corresponds to a multicomponent near vacuum problem with two rarefaction waves, while RP4 consists in a stationary contact wave.

We observe that the shock and contact waves are well captured and only some spurious oscillations of small amplitude are observed in RP2 which also exhibits a train of oscillations at the tail of the rarefaction wave. Positivity of the density is preserved in the near vacuum region which highlights the robustness of the scheme. Finally, the stationary contact wave in RP4 is exactly resolved

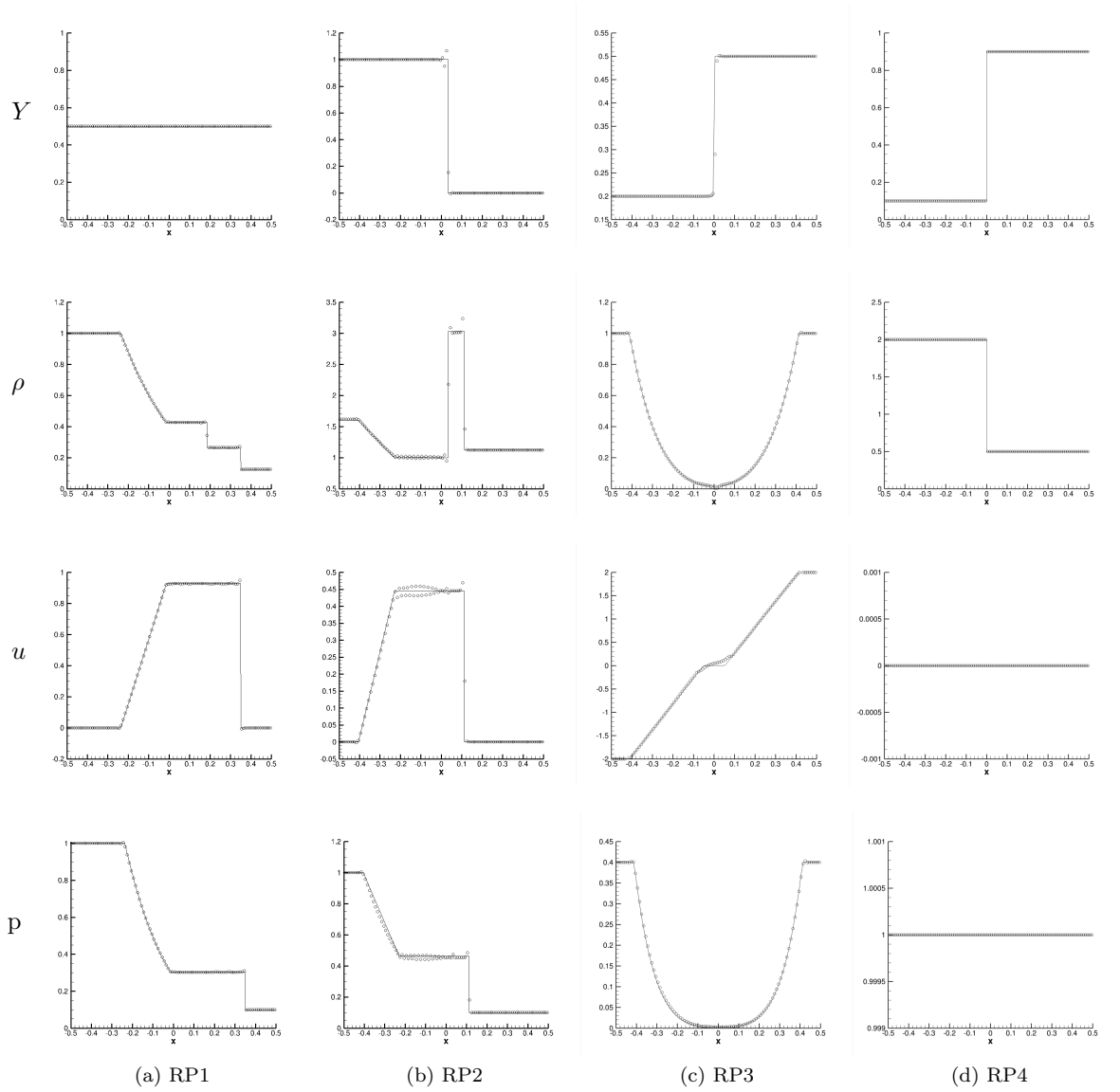


FIG. 3. Riemann problems discretized with a polynomial degree $p = 3$ and $N = 100$ cells.

as expected from [Theorem 9](#). This latter feature can also be related to the accurate resolution of the contact wave in RP1 and material interfaces in RP2 and RP3.

7.2. Shock wave-hydrogen bubble interaction. We now consider the interaction problem of a shock with a Helium bubble [28] which is commonly used to assess the resolution by numerical schemes of shock waves, material interfaces and their interaction in multiphase and multicomponent flows (see [36, 21, 42, 7] and references therein).

The domain extends to $\Omega = [0, 6.5] \times [0, 0.89]$. A left moving $M = 1.22$ normal shock wave in air is initially located at $x = 4.5$ and interacts with a bubble of helium of unit diameter with center located at $x = 3.5$ and $y = 0$. Symmetry conditions are set to the top and bottom boundaries, while non reflecting conditions are applied to the left and right limits of the domain. The thermodynamical parameters of helium and air are $\gamma_1 = 1.648$, $C_{v_1} = 6.89$ and $\gamma_2 = 1.4$, $C_{v_2} = 1.7857$, respectively. Data are made nondimensional with the initial bubble diameter and pre-shock density, temperature and sound speed. The mesh consists in a Cartesian grid with 1300×178 elements. The complete setup of the initial condition can be found in [36]. Note that this test case is usually computed including viscous effects. To avoid spurious oscillations at material interfaces in inviscid computations we regularize the initial condition of the bubble-air interface following [2, 36, 31].

Figure 4 displays contours of pressure, void fraction and numerical Schlieren obtained at different times initialized when the shock wave reaches the bubble. The shock and material discontinuities are well resolved and the solution does not present significant spurious oscillations. The results are in good qualitative agreement with the experiment in [28] and numerical simulations (see e.g., [36]). In particular the shock dynamics and the bubble deformation are well reproduced, and vortices are generated along the bubble interface due to the Kelvin-Helmholtz instability.

7.3. Richtmeyer-Meshkov instability. We now simulate the interaction of a Mach 1.21 shock wave in a mixture of air and acetone vapor with a perturbed interface separating the mixture from a dense SF6 gas [5]. The complete setup may be found in [31, 40, 38, 7]. The thermodynamical parameters of the mixture and SF6 are $\gamma_1 = 1.24815$, $C_{v_1} = 3.2286$ and $\gamma_2 = 1.0984$, $C_{v_2} = 2.0019$, respectively. The Atwood number of the initial state is $At = \frac{\rho_2 - \rho_1}{\rho_1 + \rho_2} = 0.6053$ where $\rho_2 = \gamma_2$ is taken as the pre-shock density of the mixture. Data are made nondimensional with a length scale of 1cm, and the pre-shock pressure, temperature and sound speed of the mixture. The size of the domain is $\Omega = [0, 80.1] \times [0, 5.9]$, symmetry conditions are set to the top and bottom boundaries, while non reflecting and reflecting conditions are applied to the left and right boundaries, respectively. We use a Cartesian grid with 1601×118 elements which corresponds to 118 elements per perturbation wavelength and constitutes a coarse mesh compared to other experiments [31, 40, 7].

We consider the single-mode perturbation of the material interface [5]. The shock travels to the right and interacts with the interface, then reflects at the right boundary and interacts a second time with the interface (re-shock regime). Figure 5 shows results before and after re-shock where the density and vorticity contours are displayed. The first interaction produces vorticity at the interface and the formation and roll-up of spikes, while the second interaction with the reflected shock wave produces complex fine flow field structures and a low Mach number flow field. Again, we observe a good resolution of the shock and material interface and the associated vortical structures.

8. Concluding remarks. A high-order, entropy stable and positive scheme with sharp resolution of material interfaces is introduced in this work for the discretization of a multicomponent compressible flow model in multiple space dimensions. We consider the multicomponent compressible Euler system for a mixture of two immiscible fluids that modelizes the flow of separated phases in kinematic, mechanical, and thermal equilibria. The space discretization relies on the entropy stable DGSEM framework [8, 23, 14] based on the modification of the integral over discretization elements where we replace the physical fluxes by entropy conservative numerical fluxes [51] and on the use of entropy stable numerical fluxes at element interfaces.

We propose two-point entropy conservative and entropy stable fluxes for the multicomponent flow model. The former numerical fluxes are obtained by using the Tadmor's entropy conservation condition [51]. The latter are derived from the pressure relaxation scheme for the compressible

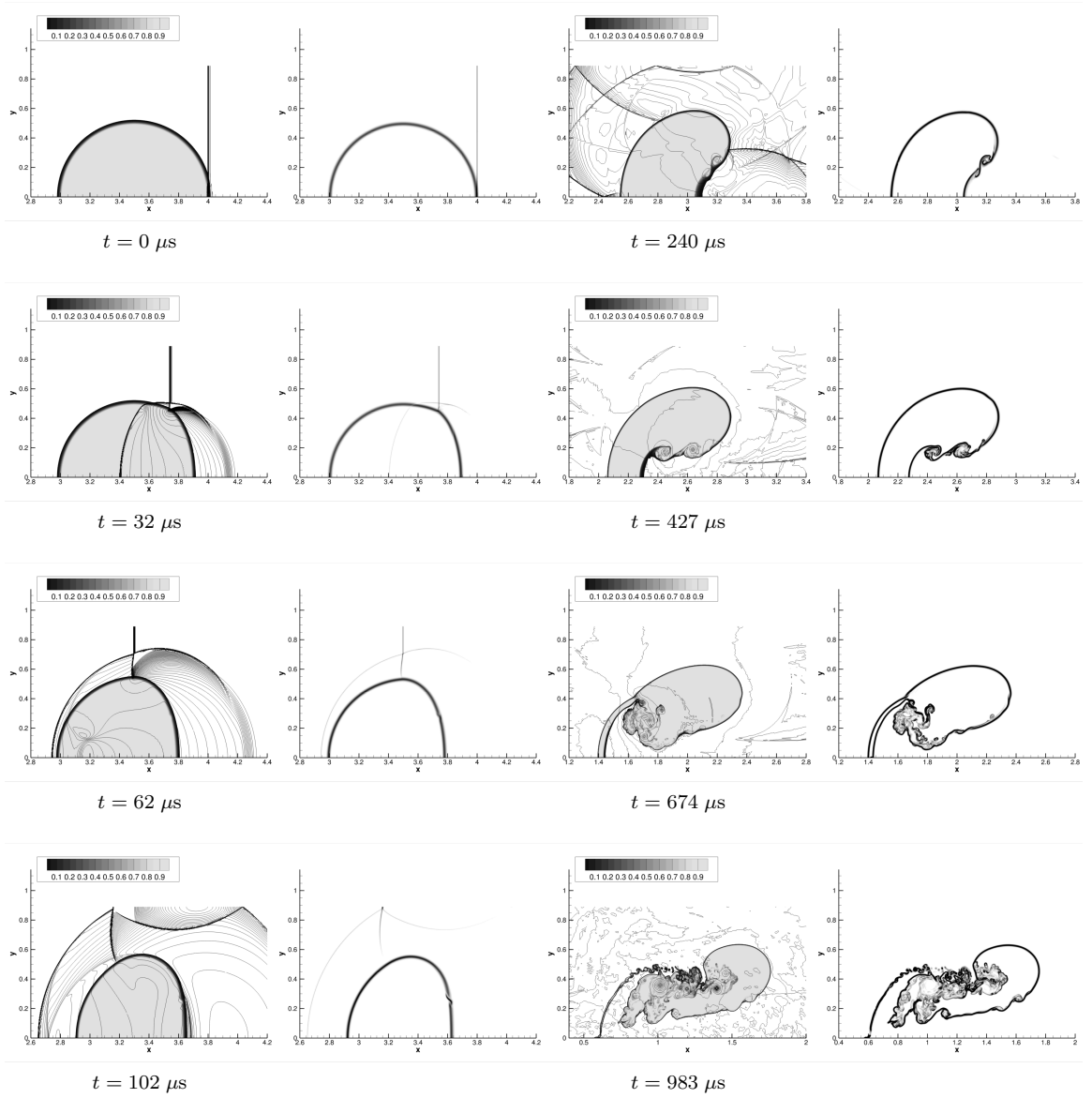


FIG. 4. *Shock wave-Helium bubble interaction: 70 pressure contours (lines) and 49 void fraction contours (colors), and Schlieren $|\nabla\rho|/\rho$ obtained with a polynomial degree $p = 3$ and a $h = 1/200$ mesh.*

Euler equations [4] and the energy relaxation approximation from [17] to allow the use of a simple polytropic equation of states for the mixture in the numerical approximation. We first derive a three-point scheme which is then used as a building block for the design of the DGSEM. Using a forward Euler discretization in time, we design a posteriori limiters and propose conditions on the numerical parameters and the time step to guaranty positivity of the solution. The scheme is also

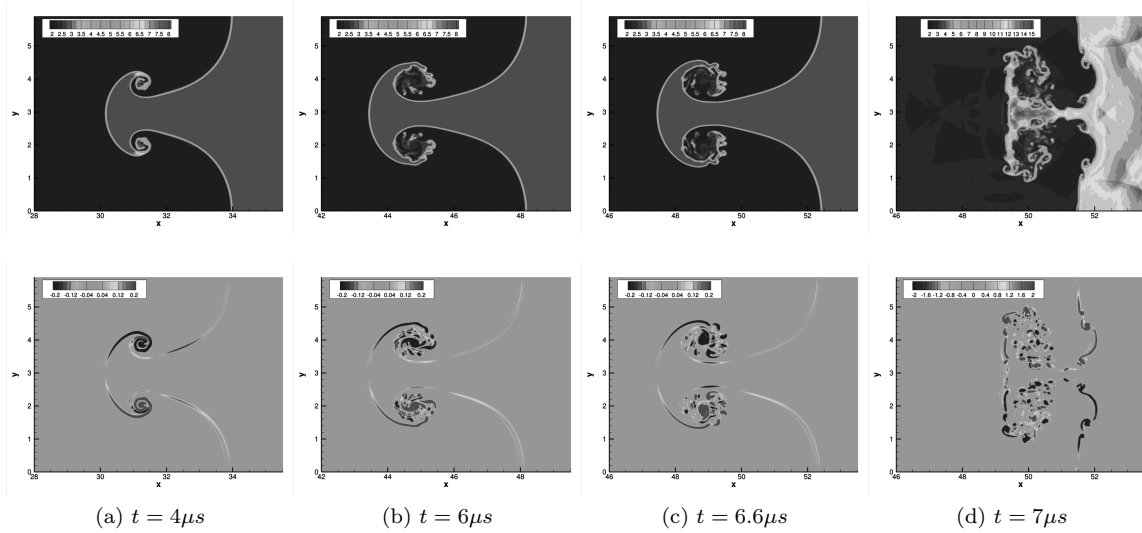


FIG. 5. *Richtmyer-Meshkov instability: density ρ (top) and vorticity $\nabla \times \mathbf{v}$ (bottom) contours before (a-c) and after (d) re-shock obtained with a polynomial degree $p = 3$ and a $h = 1/20$ mesh.*

proved to exactly resolve stationary contact waves. An explicit Runge-Kutta scheme [50] is used for the high-order time integration.

Numerical simulation of flows in one and two space dimensions with discontinuous solutions and complex wave interactions are performed with a fourth-order accurate scheme. The results highlight the accurate resolution of material interfaces, shock and contact waves, their interactions and associated small scale features. Likewise, robustness and nonlinear stability of the scheme are confirmed. Finally, we stress that the results of this work may be obviously applied to the polytropic gas dynamics for a single component.

REFERENCES

- [1] Z. Bilicki and J. Kestin, Physical aspects of the relaxation model in two-phase flow, Proc. R. Soc. Lond. A, 428 (1990), pp. 379-397.
- [2] G. Billet, V. Giovangigli, and G. de Gassowski, Impact of volume viscosity on a shock-hydrogen-bubble interaction, Combustion Theory and Modelling, 12 (2008), pp. 221-248.
- [3] M. Bohm, A. R. Winters, G. J. Gassner, D. Derigs, F. Hindenlang, and J. Saur, An entropy stable nodal discontinuous Galerkin method for the resistive MHD equations. Part I: Theory and Numerical Verification, J. Comput. Phys, 2018, <https://doi.org/10.1016/j.jcp.2018.06.027>.
- [4] F. Bouchut, Nonlinear Stability of Finite Volume Methods for Hyperbolic Conservation Laws and Well-Balanced Schemes for Sources, Frontiers in Mathematics, Birkhauser, 2004.
- [5] M. Brouillette and B. Sturtevant, Experiments on the Richtmyer-Meshkov instability: single-scale perturbations on a continuous interface. J. Fluid Mech., 263 (1994), pp. 271-292.
- [6] C. Calgari, E. Creusé, T. Goudon, and Y. Penel, Positivity-preserving schemes for Euler equations: Sharp and practical CFL conditions, J. Comput. Phys, 234 (2013), pp. 417-438.
- [7] M. Capuano, C. Bogey, and P.D.M. Spelt, Simulations of viscous and compressible gas-gas flows using high-order finite difference schemes, J. Comput. Phys, 361 (2018), pp. 56-81.
- [8] M. H. Carpenter and T. C. Fisher, High-order entropy stable finite difference schemes for nonlinear conservation laws: Finite domains, J. Comput. Phys., 252 (2013), pp. 518-557.

- [9] M. H. Carpenter, T. C. Fisher, E. J. Nielsen, and S. H. Frankel, Entropy stable spectral collocation schemes for the Navier-Stokes equations: discontinuous interfaces, *SIAM J. Sci. Comput.*, 36 (2014), pp. B835–B867.
- [10] C. Chalons and J. F. Coulombel, Relaxation approximation of the Euler equations, *J. Math. Anal. Appl.*, 348 (2008), pp. 872–893.
- [11] P. Chandrashekar, Kinetic energy preserving and entropy stable finite volume schemes for compressible Euler and Navier-Stokes equations, *Commun. Comput. Phys.*, 14 (2013); pp. 1252–1286.
- [12] J.-B. Chapelier, M. de la Llave Plata, F. Renac, and E. Lamballais, Evaluation of a high-order discontinuous Galerkin method for the DNS of turbulent flows, *Comput. Fluids*, 95, (2014), pp. 210–226.
- [13] G.-Q. Chen, C. D. Levermore, and T.-P. Liu, Hyperbolic Conservation Laws with Stiff Relaxation Terms and Entropy, *Comm. Pure Appl. Math.*, 47 (1994), pp. 787–830.
- [14] T. Chen and C.-W. Shu, Entropy stable high order discontinuous Galerkin methods with suitable quadrature rules for hyperbolic conservation laws, *J. Comput. Phys.*, 345 (2017), pp. 427–461.
- [15] F. Coquel, E. Godlewski, A. In, B. Perthame, and P. Rascle, Some new Godunov and relaxation methods for two-phase flow problems. Godunov methods, Kluwer/Plenum, New York, 2001, pp. 179–188.
- [16] F. Coquel, C. Marmignon, P. Rai, and F. Renac, An entropy stable high-order discontinuous Galerkin spectral element method for the Baer-Nunziato model, submitted, 2019.
- [17] F. Coquel and B. Perthame, Relaxation of energy and approximate Riemann solvers for general pressure laws in fluid dynamics, *SIAM J. Numer. Anal.*, 35 (1998), pp. 2223–2249.
- [18] S. Dellacherie, Relaxation schemes for the multicomponent Euler system, *ESAIM: Math. Model. and Numer. Analysis (M2AN)*, 37 (2003), pp. 909–936.
- [19] B. Després, Entropy inequality for high order discontinuous Galerkin approximation of Euler equations, in VII conference on hyperbolic problems. ETHZ-Zurich, 1998.
- [20] B. Després, Discontinuous Galerkin method for the numerical solution of Euler equations in axisymmetric geometry, in B. Cockburn, G. E. Karniadakis and C.-W. Shu (Eds.), *Discontinuous Galerkin Methods: Theory, Computation and Applications*, Lecture Notes in Computational Science and Engineering, 11 (2000), Springer-Verlag, pp. 315–320.
- [21] R. P. Fedkiw, T. Aslam, B. Merriman, and S. Osher, A non-oscillatory Eulerian approach to interfaces in multimaterial flows (the ghost fluid method), *J. Comput. Phys.*, 152 (1999), pp. 457–492.
- [22] U. S. Fjordholm, S. Mishra, and E. Tadmor, Arbitrarily high-order accurate entropy stable essentially nonoscillatory schemes for systems of conservation laws, *SIAM J. Numer. Anal.*, 50 (2012), pp. 544–573.
- [23] G. J. Gassner, A Skew-symmetric discontinuous Galerkin spectral element discretization and its relation to SBP-SAT finite difference methods, *SIAM J. Sci. Comput.*, 2013 (35), pp. A1233–A1253.
- [24] G. J. Gassner, A. R. Winters, and D. A. Kopriva, Split form nodal discontinuous Galerkin schemes with summation-by-parts property for the compressible Euler equations, *J. Comput. Phys.*, 327 (2016), pp. 39–66.
- [25] E. Godlewski and P.-A. Raviart, *Numerical Approximation of Hyperbolic Systems of Conservation Laws*, Springer, 1986.
- [26] A. Harten and P. D. Lax, A random choice finite difference scheme for hyperbolic conservation laws, *SIAM J. Numer. Anal.*, 18 (1981), pp. 289–315.
- [27] A. Harten, P. D. Lax, and B. Van Leer, On upstream differencing and Godunov-type schemes for hyperbolic conservation laws, *SIAM Rev.*, 25 (1983), pp. 35–61.
- [28] J. F. Hass and B. Sturtevant, Interaction of weak shock waves with cylindrical and spherical gas inhomogeneities, *J. Fluid Mech.*, 181 (1987), pp. 41–76.
- [29] M. T. Henry de Frahan, S. Varadan, and E. Johnsen, A new limiting procedure for discontinuous Galerkin methods applied to compressible multiphase flows with shocks and interfaces, *J. Comput. Phys.*, 280 (2015), pp. 89–509.
- [30] A. Hildebrand and S. Mishra, Entropy stable shock capturing space-time discontinuous Galerkin schemes for systems of conservation laws, *Numer. Math.*, 126 (2014), pp. 103–151.
- [31] R. W. Houim and K. K. Kuo, A low-dissipation and time-accurate method for compressible multi-component flow with variable specific heat ratios, *J. Comput. Phys.*, 230 (2011), pp. 8527–8553.
- [32] F. Ismail and P. L. Roe, Affordable, entropy-consistent Euler flux functions II: Entropy production at shocks, *J. Comput. Phys.*, 228 (2009), pp. 5410–5436.
- [33] G. Jiang and C.-W. Shu, On a cell entropy inequality for discontinuous Galerkin methods, *Math. Comput.*, 62 (1994), pp. 531–538.
- [34] S. Jin and Z. P. Xin, The relaxation schemes for systems of conservation laws in arbitrary space dimension, *Comm. Pure Appl. Math.*, 48 (1995), pp. 235–276.
- [35] E. Johnsen and T. Colonius, Implementation of WENO schemes in compressible multicomponent flow problems, *J. Comput. Phys.*, 219 (2006), pp. 715–732.

- [36] S. Kawai and H. Terashima, A high-resolution scheme for compressible multicomponent flows with shock waves, *Int. J. Numer. Meth. Fluids*, 66 (2011), pp. 1207–1225.
- [37] D. A. Kopriva and G. Gassner, On the quadrature and weak form choices in collocation type discontinuous Galerkin spectral element methods, *J. Sci. Comput.*, 44 (2010), pp. 136–155.
- [38] M. Latini, O. Schilling, and W. S. Don, Effects of WENO flux reconstruction order and spatial resolution on reshocked two-dimensional Richtmyer-Meshkov instability, *J. Comput. Phys.*, 221 (2007), pp. 805–836.
- [39] R. C. Moura, G. Mengaldo, J. Peiró, and S. J. Sherwin, On the eddy-resolving capability of high-order discontinuous Galerkin approaches to implicit LES / under-resolved DNS of Euler turbulence, *J. Comput. Phys.*, 330 (2017), pp. 615–623.
- [40] P. Movahed and E. Johnsen, A solution-adaptive method for efficient compressible multifluid simulations, with application to the Richtmyer-Meshkov instability, *J. Comput. Phys.*, 239 (2013), pp. 166–186.
- [41] B. Perthame and C.-W. Shu, On positivity preserving finite volume schemes for Euler equations, *Numer. Math.*, 73 (1996), pp. 119–130.
- [42] J. J. Quirk and S. Karni, On the dynamics of a shock-bubble interaction, *J. Fluid Mech.*, 318 (1996), pp. 129–163.
- [43] J. Qiu, B. C. Khoo, and C.-W. Shu, A numerical study for the performance of the Runge-Kutta discontinuous Galerkin method based on different numerical fluxes, *J. Comput. Phys.*, 26 (2006), pp. 540–565.
- [44] F. Renac, Stationary discrete shock profiles for scalar conservation laws with a discontinuous Galerkin method, *SIAM J. Numer. Anal.*, 53 (2015), pp. 1690–1715.
- [45] F. Renac, M. de la Llave Plata, E. Martin, J.-B. Chapelier, and V. Couaillier, Aghora: A high-order DG solver for turbulent flow simulations, in N. Kroll, C. Hirsch, F. Bassi, C. Johnston and K. Hillewaert (Eds.), *IDIHOM: Industrialization of High-Order Methods - A Top-Down Approach*, Notes on Numerical Fluid Mechanics and Multidisciplinary Design, 128 (2015), Springer Verlag.
- [46] F. Renac, A robust high-order Lagrange-projection like scheme with large time steps for the isentropic Euler equations, *Numer. Math.*, 135 (2017), pp. 493–519.
- [47] F. Renac, A robust high-order discontinuous Galerkin method with large time steps for the compressible Euler equations, *Commun. Math. Sci.*, 15 (2017), pp. 813–837.
- [48] F. Renac, Entropy stable DGSEM for nonlinear hyperbolic systems in nonconservative form with application to two-phase flows. *J. Comput. Phys.*, 382 (2019), pp. 1–26.
- [49] R. Saurel and C. Pantano, Diffuse-interface capturing methods for compressible two-phase flows, *Annu. Rev. Fluid Mech.*, 50 (2018), pp. 105–30.
- [50] C.-W. Shu and S. Osher, Efficient implementation of essentially non-oscillatory shock-capturing schemes, *J. Comput. Phys.*, 77 (1988), pp. 439–471.
- [51] E. Tadmor, The numerical viscosity of entropy stable schemes for systems of conservation laws. I, *Math. Comput.*, 49 (1987), pp. 91–103.
- [52] E. Tadmor, Entropy stability theory for difference approximations of nonlinear conservation laws and related time-dependent problems, *Acta Numer.*, 12 (2003), pp. 451–512.
- [53] F. Vilar, C.-W. Shu, and P.-H. Maire, Positivity-preserving cell-centered Lagrangian schemes for multi-material compressible flows: From first-order to high-orders. Part II: The two-dimensional case, *J. Comput. Phys.*, 312 (2016), pp. 416–442.
- [54] N. Wintermeyer, A. R. Winters, G. J. Gassner, and D. A. Kopriva, An entropy stable nodal discontinuous Galerkin method for the two dimensional shallow water equations on unstructured curvilinear meshes with discontinuous bathymetry, *J. Comput. Phys.*, 340 (2017), pp. 200–242.
- [55] A. R. Winters, D. Derigs, G. J. Gassner, and S. Walch, A uniquely defined entropy stable matrix dissipation operator for high Mach number ideal MHD and compressible Euler simulations, *J. Comput. Phys.*, 332 (2017), pp. 274–289.
- [56] T. Xiong, C.-W. Shu, and M. Zhang, WENO scheme with subcell resolution for computing nonconservative Euler equations with applications to one-dimensional compressible two-medium flows, *J. Sci. Comput.*, 53 (2012), pp. 222–247.
- [57] X. Zhang and C.-W. Shu, On positivity-preserving high order discontinuous Galerkin schemes for compressible Euler equations on rectangular meshes, *J. Comput. Phys.*, 229 (2010), pp. 8918–8934.